Materials Today Bio 28 (2024) 101213

Contents lists available at ScienceDirect

Materials Today Bio

journal homepage: www.journals.elsevier.com/materials-today-bio

Magnetic stirring with iron oxide nanospinners accretes neurotoxic $A\beta_{42}$ oligomers into phagocytic clearable plaques for Alzheimer's disease treatment

Arjun Sabu [a,1], Yu Ching Huang [b,c,1], Ramalingam Sharmila [a], Chih-Yuan Sun [a], Min-Ying Shen [a,d,**], Hsin-Cheng Chiu [a,*]

[a] Department of Biomedical Engineering and Environmental Sciences, National Tsing Hua University, Hsinchu City, Taiwan
[b] Department of Neurology, Taoyuan General Hospital, Ministry of Health and Welfare, Taiwan
[c] Department of Industrial Engineering and Management, Yuan-Ze University, Taoyuan City 320315 Taiwan
[d] Department of Surgery, China Medical University Hsinchu Hospital, Hsinchu County 30272, Taiwan

ARTICLE INFO

Keywords:
Alzheimer's disease
β-Amyloid 42 oligomers
Superparamagnetic iron oxide nanoparticles
Nanoscaled stirring treatment
Microglial cell polarization
Phagocytic clearance

ABSTRACT

An increasing number of medications have been explored to treat the progressive and irreversible Alzheimer's disease (AD) that stands as the predominant form of dementia among neurodegenerative ailments. However, assertions about toxic side effects of these drugs are a significant hurdle to overcome, calling for drug-free nanotherapeutics. Herein, a new therapeutic strategy devoid of conventional drugs or other cytotoxic species was developed. The constructed superparamagnetic iron oxide nanoparticles (SPIONs) nanospinners can accrete neurotoxic β-amyloid 42 oligomers ($oA\beta_{42}$) into aggregated magnetic plaques (mpAβ) by mechanical rotating force via remote interaction between nanoparticles and the applied magnetic field. While the cellular uptake of mpAβ attained from the magnetic stirring treatment by neuronal cells is severely limited, the facile phagocytic uptake of mpAβ by microglial cells leads to the polarization of the brain macrophages to M2 phenotype and thus the increased anti-inflammatory responses to the treatment. The SPION stirring treatment protects the AD mice from memory deterioration and maintain cognitive ability as evidenced from both nesting and Barnes maze tests. The examination of the $oA\beta_{42}$ injected brain tissues with the stirring treatment showed significant amelioration of functional impairment of neurons, microglia, astrocytes and oligodendrocytes alongside no obvious tissue damage caused by stirring meanwhile complete degradation of SPION was observed at day 7 after the treatment. The in vitro and animal data of this work strongly corroborate that this new modality of undruggable stirring treatment with SPIONs provides a new feasible strategy for developing novel AD treatments.

1. Introduction

Alzheimer's disease (AD) is the most prevalent type of dementia among neurodegenerative disorders, with a recent increase in mortality rate as a consequence of AD being a COVID-19 comorbidity [1,2]. The Dementia Forecasting Collaborators (2022) estimate that the overall predicted dementia incidence in the global population will reach 152.8 million by 2050 [3]. The amyloid cascade hypothesis suggests that β-amyloid 42 oligomers ($oA\beta_{42}$) are the primary toxic species. Its over-accumulation within neuronal cells has been recognized as a critical intermediate step in AD-related irregularities [4–6]. The binding of $oA\beta_{42}$ to the plasma membranes of neuronal cells triggers transmembrane signalling and intracellular changes, leading to synaptic failure and, ultimately, cognitive impairment [7,8].

The predominant activity modulation of microglia/macrophages by soluble Aβ oligomers and protofibrillar species is an essential element in AD histopathology [9]. Studies have shown that the microglia/macrophages are plastic cells and can undertake different phenotypes and display distinct activity and functional performances [10,11]. Emerging evidence corroborates the critical role of $oA\beta_{42}$ to induce

* Corresponding author.
** Corresponding author. Department of Biomedical Engineering and Environmental Sciences, National Tsing Hua University, Hsinchu City, Taiwan.
E-mail addresses: mingyin.shen@gmail.com (M.-Y. Shen), hscchiu@mx.nthu.edu.tw (H.-C. Chiu).
[1] The authors contribute to this work equally.

https://doi.org/10.1016/j.mtbio.2024.101213
Received 19 June 2024; Received in revised form 15 August 2024; Accepted 23 August 2024
Available online 27 August 2024

inflammation in AD pathogenesis, including tau aggregation and phosphorylation, neuronal inflammation, neurodegeneration, synaptic dysfunction and cognitive impairment [9–12]. The prolonged activation of microglia steers the process to induce aggregation of $A\beta_{42}$ into oligomers and fibrils by triggering pro-inflammatory cytokines and other signalling pathways, which subsequently contribute to neuronal damage and losses. M2 phenotype microglial cells can exclude aggregated Aβ species owing to their exceptional phagocytic capability compared to M1 microglial cells, astrocytes, and immune cells in the central nervous system (CNS) [12,13]. Besides, the M2 microglial cells secrete neurotrophic factors and anti-inflammatory cytokines in the brain. This further aids the repair of CNS damage and relieves inflammation [14,15]. Although the ability of infiltrating M2-like cells to eliminate the Aβ species and mitigate AD-induced cognitive impairment has been recognized, unfortunately, naive microglial cells in neuroinflammatory regions differentiate mostly into the M1 phenotype along with inflammation be further intensified [16–18].

Several drugs have been approved by the U.S. Food and Drug Administration to help manage symptoms in people with AD. However, none of the therapies clinically available have been reported to cure AD. Moreover, most therapeutically approved drugs showed significant side effects due to their dosages. Extensive research attempting to contemplate the pathophysiology of AD with development of advanced therapeutics has remained elusive. The efficacy of previously proposed therapeutic strategies like secretase 1 (beta-site amyloid precursor protein cleaving enzyme-1) inhibition and passive anti-amyloid-immunotherapies was not pronounced, probably due to their poor efficiency in eliminating the $oA\beta_{42}$ species from the brain [19,20]. Nanotechnology has appeared as an alternative way to treat AD, compared to conventional drugs alone. Hu and his research group used chiral L- and D-glutathione stabilized gold nanoparticles to protect tissues from damage caused by reactive oxygen species (ROS) and inhibit Aβ aggregation in vitro [21]. Zhang and Park developed ROS generation nanoparticles (NPs) to induce cleavage of Aβ aggregates with a low-frequency magnetic field into oxidized nontoxic species [22]. It is noteworthy that these strategies focused only and mainly on elimination of Aβ plaques. However, because $oA\beta_{42}$ and fibrillar species are the key elements in charge of the neurotoxicity, attentions should be paid to remove $oA\beta_{42}$ rather than Aβ plaques. Furthermore, ROS generation is not a pertinent solution for AD treatment as high levels of ROS accumulation are intimately associated with impairments in cognitive function and synaptic plasticity [23]. A new strategy with drug- and ROS-free therapeutics is thus in great demand to capture and remove $oA\beta_{42}$ from the AD brain without affecting the functions of neuronal cells.

Recently, AuNPs were fabricated by citrate reduction and adopted for adsorption of Aβ oligomers on nanoparticle surfaces, leading to the formation of amyloid surface corona serving as a screening platform for AD drug discovery [24]. Due to electrostatic and solvation forces, the negatively charged AuNPs accelerate the immobilization of amyloids on their surface by interacting with the N terminal end of the Aβ monomer, thus facilitating formation of Aβ oligomer coronas. In our previous work, we introduced a silica-coated microscale iron oxide stir bar (MSB) for rapid accretion of $oA\beta_{42}$ into large magnetic aggregates (mpAβ) and inhibits neuroinflammation [25]. However, laborious and time-consuming preparation work was required along with a large size distribution of MSB being usually observed. Utilizing micro-sized magnetic materials to generate mechanical force shows possible mechanical destruction of cell membrane integrity [26,27]. Challenges with the MSB therapy for the AD treatment also include administration and slow bio-elimination for clinical applications. Unlike microsized stir bars, superparamagnetic nanoparticles exhibit high mobility in body tissues due to their high surface area-to-volume ratio. Therefore, magnetic particles in nanoscale (<50 nm in diameter) such as superparamagnetic iron oxide nanoparticles (SPIONs) have received considerable interests in diagnosing and treating AD due to their potential properties [28–31].

Herein, citric acid-coated iron oxide NPs with excellent paramagnetic properties and biocompatibility were constructed and adopted as a nanospinner system in combination with facile magnetic rotation field to efficiently capture neurotoxic soluble $oA\beta_{42}$ via magnetic stirring treatment. The effect of the stirring treatment with SPIONs as nanospinners under magnetic field on accreting highly neurotoxic $oA\beta_{42}$ species into magnetic plaques was evaluated in situ and the variance in the cytotoxicity and cellular function impairment between $oA\beta_{42}$ and magnetic plaques toward neurons and microglia was thoroughly examined. The alleviation of the learning and memory deterioration caused by the intracranial injection of $oA\beta_{42}$ species in brain (hippocampus) in mice after receiving the SPION stirring treatment was evaluated in vivo by both the nesting and Barnes maze tests. To validate the therapeutic efficacy and the biosafety of the magnetic NPs with stirring treatment, the brain tissue sections were examined by various IHC staining to separately evaluate the cellular functions and important protein marker expression of neurons, microglia, astrocytes and oligodendrocytes after the stirring treatment. The H&E staining of brain tissues receiving the stirring treatment and the degradation of SPION in tissues with time was examined. This new drug-free therapeutic strategy did not induce neurotoxicity or activate pro-inflammatory microglia in the brain tissues due to the lack of drug-induced ROS generation and cytotoxicity. Furthermore, magnetic stimulation therapy rescued the AD-like mice from memory and cognitive impairment induced by $oA\beta_{42}$. Despite the formation of non-pathogenic magnetic Aβ plaques, these aggregated species were eliminated by microglia via phagocytosis. This study strongly suggests that the magnetic stirring treatment with SPIONs can be highly potential as a plausible treatment against AD by capturing and accretion of toxic $oA\beta_{42}$ species. The primary strategy for capturing and accumulating cytotoxic $oA\beta_{42}$ species into magnetic plaques and its phagocytic clearance is illustrated in Fig. 1.

2. Materials and methods

2.1. Materials and Reagents

Iron trichloride hexahydrate ($FeCl_3$. $6H_2O$), sodium oleate, citric acid, Congo red (CR), thioflavin T (ThT), and haematoxylin and eosin (H&E) were purchased from Sigma-Aldrich. $A\beta_{42}$ peptide was purchased from GL Biochem. 1,1,1,3,3,3-hexafluoro-2- propanol (HFIP) was purchased from Alfa Aesar. Dulbecco's modified Eagle's medium (DMEM), Hoechst 33258, Rabbit anti IBA1 (PA5-27436), Rabbit anti-CD68 (14-0681-82) and Goat anti-Rabbit Alexa Fluor 488 (A-11008) were purchased from Invitrogen, Rabbit anti-beta Amyloid antibody (ab2539). Rabbit anti-EAAT2 (ab41621), Chicken anti-MBP (ab40390), Goat anti Rabbit FITC (ab97050), Goat anti-Mouse FITC (ab97022), Goat Anti-Chicken antibody Alexa Fluor® 647 (ab150171) and Goat Anti-Mouse antibody Alexa Fluor® 647 (ab150115) and F-actin staining kit (ab112125) were purchased from Abcam. ECL Substrate kit (APL-1023) was purchased from APOLO Biochemical. Anti-human β-amyloid (6E10) antibody were purchased from BioLegend. Chicken anti-MAP2 antibody (ARG52328), Rabbit anti-Caspase 3 (ARG54938), Anti-F-actin antibody (ARG23737), Mouse anti-beta III Tubulin antibody (ARG62683), Goat anti-Rabbit Texas Red (ARG21727) Mouse anti-GFAP (ARG10122), Goat anti-Chicken FITC (ARG65603) were purchased from Arigo biolaboratories. N2a (murine neuroblastoma cells) and BV-2 (murine microglial cells) were obtained from Food Industry Research and Development Institute (Hsinchu City, Taiwan).

2.2. Synthesis and characterizations of OA-SPIONs and CA-SPIONs

Oleic acid-modified superparamagnetic iron oxide nanoparticles (OA-SPIONs) were synthesized by the thermal decomposition method as reported previously [32]. In brief, 9 mL of deionized water, 12 mL ethanol, and 21 mL n-hexane were mixed in a round bottom flask. 1.62 g of $FeCl_3.6H_2O$ and 5.475 g of sodium oleate were added. The solution was heated under reflux for 4 h in an oil bath at 69 °C. After heating, the

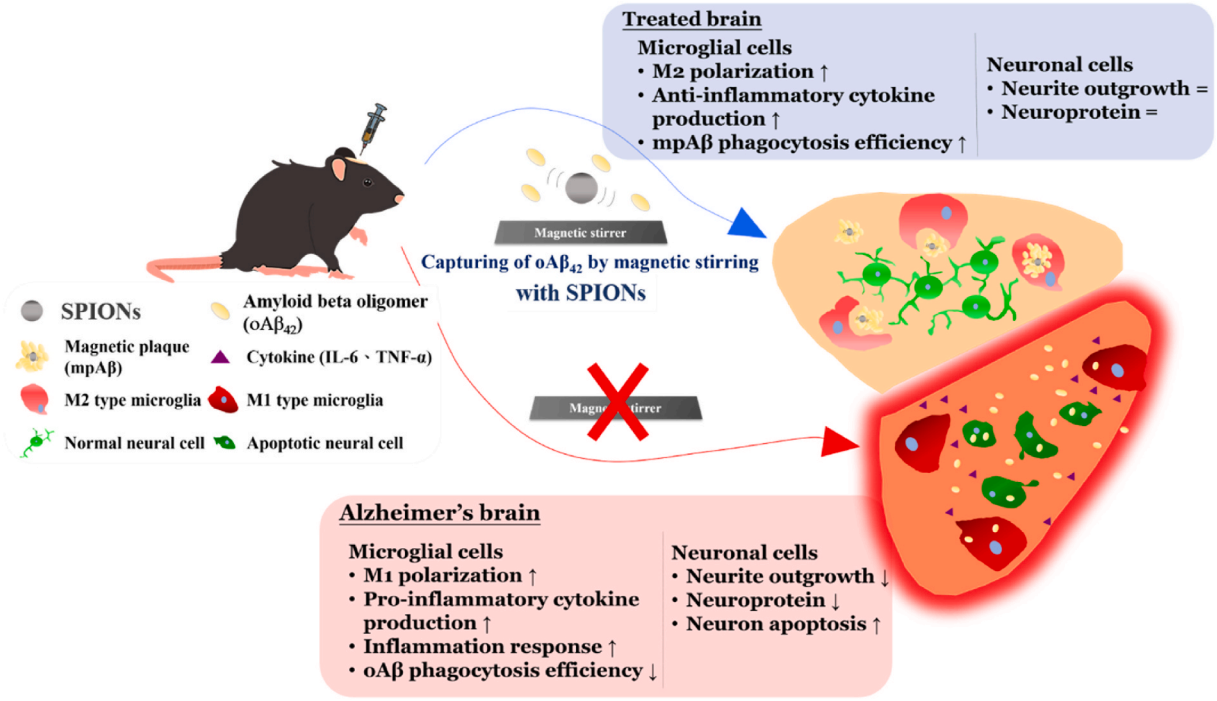

Fig. 1. Schematic illustration of effective therapeutic action of SPIONs by accreting cytotoxic oAβ_{42} species into magnetic plaques and enhancing cellular clearance by microglial cells for the treatment of AD.

upper reddish-brown solution was purified by repeated extraction with DI water to remove excess unreacted sodium oleate. Hexane was then removed by rotary evaporator. Iron oleate precursor as a dark brown liquid was thus obtained. Iron oleate precursor (3.6 g) and oleic acid (0.64 mL) were added into tri-n-octylamine (25.3 mL). The reaction solution was heated to 80 °C for 15 min, 100 °C for 15 min, and 160 °C for 30 min to remove water under constant stirring and N_2 flow. After the removal of water, the reaction solution was heated to 340 °C with a heating rate of 3.3 °C/min and kept at that temperature for 5 h. After the reaction, ethanol/n-hexane solution (5/1 v/v) was added to the mixture. The precipitated particles were then purified by centrifugation (8000 rpm, 10 min) in the same solution and the procedure was repeated until the supernatant became colorless. The black pellets were dried in vacuo. For the preparation of citrate coated SPIONs (CA-SPIONs), OA-SPIONs (10 mg) and citric acid (10 mg) were added into dimethylformamide (3 mL) and the solution was heated at 100 °C for 24 h. Citrate coated SPIONs was precipitated from diethyl ether (8 ml) and collected by magnetic separation. The particles (CA-SPIONs, being further abbreviated as SPIONs hereinafter) were washed with acetone to remove free citric acid and collected under a permanent magnetic field.

The mean hydrodynamic diameter (D_h), size distribution (polydispersity index, PDI) and zeta potential of SPIONs were determined by dynamic light scattering (DLS, ZetaSizer Nano Series, Malvern, UK). The aqueous colloidal stability of nanoparticles was evaluated in terms of the dynamic light scattering intensity of the aqueous NP suspension at a concentration of 200 μg/mL in DIW, PBS and DMEM, respectively, at 37 °C over different time intervals (0, 30, 60, 90 and 120 min). The morphology of OA-SPIONs and SPIONs was examined with high resolution thermal field emission scanning electron microscopy (HRFEG-SEM, JSM 7610F, JEOL, Japan) and transmission electron microscope (TEM, T7700, Hitachi, Tokyo, Japan). A drop of the diluted NP suspension in hexane (OA-SPIONs) or in water (SPIONs) was placed on a carbon-coated copper grid (200 mesh copper grids, Ted Pella, Inc., Redding, CA, USA) and dried for the sample preparation with the HRFEG-SEM and TEM examination. The mean sizes of OA-SPIONs and SPIONs were calculated using ImageJ Software from the HRFEG-SEM and TEM images. A high-performance low-temperature multi-function X-ray diffractometer (Low-Temperature XRD, D8 Discover X-Ray Diffraction System, Bruker) was used to examine the crystal structure of OA-SPIONs. Characterization of superparamagnetic properties of OA-SPIONs and SPIONs was carried out on a superconducting quantum interference device (SQUID) magnetometer at 300 K (MPMS-XL Quantum Design, San Diego, CA, US). The iron oxide content of OA-SPIONs was determined by thermogravimetric analyzer by heating from 30 to 800 °C (TGA, Mettler-Toledo, Greifensee, Switzerland) at a heating rate of 10 °C min^{-1}. The stirring experiment of SPIONs in DIW was performed by addition of an aqueous CR solution (50 μM, 2 μL) into a droplet of DIW (12 μL) on a glass slide containing SPIONs at a final concentration of 14.3 μg/mL. The aqueous droplet amounting to 14 μL in total volume was subjected to magnetic stirring at 2500 rpm using IKA magnetic stirrer (big squid white, Staufen, Germany) with speed range: 0–2500 rpm. The dimensions of the magnetic stirrer are 185× 45 × 205 mm (W x D x H), with a permissible ambient temperature from 5 to 40 °C. The rotation frequency of the stirrer is 50/60 Hz. The stirring speed was calibrated using an external speed sensor that responds to magnetic impulses. The same conditions of the stirrer were maintained for all the in vivo and in vitro experiments.

2.3. Preparation and characterization of $A\beta_{42}$ species

oAβ_{42} and npAβ were prepared and characterized according to the methods described previously [33,34]. Briefly, oAβ_{42} and npAβ (naturally occurring Aβ plaques) were prepared and characterized according to the methods described previously [2–4]. To avoid pre-formation of the β-sheet structure, 4.8 mg of Aβ peptide was initially dissolved in 4.8 mL hexafluoro-2-propanol by shaking in an orbital shaking bath at 150 rpm for 4h at 4 °C. Then the solution was divided into 10 equal aliquots in low protein binding sterile 1.5 mL microcentrifuge tubes. Then the HFIP was completely removed in vacuo. The peptide film thus obtained was stored in a desiccator at −20 °C before use. When needed, 213 μL sodium hydroxide (NaOH, 2 μM) was added to the formed Aβ species (final concentration is 0.5 mM) and shaken for 5 min at 15000 rpm, 4 °C. The supernatant was centrifuged and collected, followed by the quick addition of phosphate-buffered saline (0.1M) into the supernatant and

incubated at 37 °C. The structures of oAβ_{42} were examined by ThT assay and CR dye. For the ThT assay, Aβ_{42} peptide (50 μM) and ThT (30 μM) were added into PBS (pH 7.4, 100 μL). The solution was incubated at 37 °C on a 96-well plate. As a function of time, the fluorescence intensity of ThT was determined using a microplate reader (Infinite M200, TECAN, Switzerland). The excitation was performed at 440 nm and the emission spectrum was recorded at 480 nm. Due to the formation of npAβ, the characteristic absorbance of CR dye (490 nm) showed a red shift in the range 490–540 nm and was determined using a UV/Vis spectrometer. The morphologies of oAβ_{42}, fibrils, npAβ, and other Aβ species were evaluated separately with TEM (Bio-TEM, model: HT7700, Hitachi, Japan), AFM and SPM (tapping mode, Bruker, Model-Dimension Icon, Camarillo, CA, USA). For the TEM sample preparation, Aβ (50 μM) in PBS was incubated for 0, 6, 12, 20, 24, and 120 h, respectively, at 37 °C. Then a drop of the Aβ dispersion was added onto a carbon-coated grid (200 mesh copper grids, Ted Pella, Inc., Redding, CA, USA) and dried at 25 °C. For the preparation of the AFM and SPM samples, a drop of the Aβ solution was placed on a 0.13 mm thick cover glass and dried in air. It was washed repeatedly with DIW to ensure the removal of salt and then air-dried.

2.4. Dot blot assay

A Dot blot assay was utilized to ascertain the formation of oAβ_{42} and amyloid fibrils separately by employing their corresponding antibodies, while also determining the incubation duration necessary for the formation of oAβ_{42} and amyloid fibrils in PBS at 37 °C. oAβ_{42} (50 μM) in PBS was subjected to incubation at 37 °C for various time intervals (0, 4, 8, 12, 16, 20, 24, 36, 48, 72, 96, 120, 144, 168 h) and spotted onto a nitrocellulose membrane. After being completely dried, the membrane was immersed in TBST solution (20 mM Tris-HCl, 150 mM NaCl, 0.05 % Tween 20, pH 7.5) containing 5 % bovine serum albumin (BSA) for 1 h. Then the membrane was again transferred to TBST solution containing rabbit anti-amyloid fibrils antibody (1:200) or rabbit anti-amyloid oligomers antibody (1:200) and shaken at 4 °C overnight. The membrane was then washed with TBST solution, and transferred to TBST solution containing goat anti-rabbit HRP antibody (1:200), and allowed it to stand for 1 h at room temperature (RT). Again, TBST solution was used to clean the membrane. The ECL Substrate kit was used to generate luminescence. Finally, a G-BOX multifunctional fluorescent luminescence imaging system was used to detect the luminescence on the film. The signal intensity of the luminescence was analyzed by Image-Pro Plus 6.0 software.

2.5. Accretion and aggregation of oAβ_{42} by SPION stirring treatment

In a 96-well plate, pre-cultured oAβ_{42} (25 μM) for 20 h was treated with three concentrations (0, 100, 200 μg/mL) of SPIONs. CR and ThT (both at 15 μM final concentration) were added, bringing the total volume to 100 μL. The plate was then subjected to 37 °C temperature with stirring at 2500 rpm using an electromagnetic stirrer. Rotating magnetic stirring was conducted on an IKA magnetic stirrer (big squid white, Staufen, Germany) with a glass surface. After 30 min of magnetic stirring, fluorescence microscopy was employed to observe CR red fluorescence (ex: 576 nm, em: 614 nm) and ThT fluorescence (ex: 442 nm, em: 485 nm), evaluating the efficacy of SPIONs at different concentrations in stirring and aggregating oAβ_{42}. The morphology of mpAβ as well as the oAβ_{42} without SPIONs treatment were examined by Bio TEM (HT7700, Hitachi, Japan), SPM and AFM (tapping mode, Bruker, Model-Dimension Icon, Camarillo, CA, USA).

2.6. Cell lines used and cell culture

(1) Neuro-2a (N2a) cells are mouse neuroblasts with neuronal and amoeboid stem cell morphology isolated from brain tissue of C57BL/6 strain. The cells were cultured in DMEM (High Glucose, 12100-046, Gibco) containing 10 % fetal bovine serum (FBS), 1 % penicillin/streptomycin, 1 mM sodium pyruvate, and placed at 37 °C, 5 % CO_2 sterile in the incubator.

(2) BV-2 (mouse, brain, microglial cells) cells are mouse glial cells of the C57BL/6 strain. The cells were cultured in DMEM (High Glucose, 12100-046, Gibco) containing 10 % FBS and 1 % Penicillin/Streptomycin, and placed in a sterile incubator at 37 °C and 5 % CO_2.

2.7. Cell viability of N2a cells treated with SPION stirring treatment and with oAβ_{42}

The MTT assay was used to determine the cell viability of N2a cells incubated with SPIONs. N2a cells (1.5×10^4 cells/well) in DMEM (high glucose, 1 % FBS, without phenol red) were cultured in a 96-well plate over 24 h. After 24 h of incubation, different concentrations of SPIONs were added (0, 50, 100, 150, 200 μg/mL) into the cell culture medium, and then electromagnetic stirring (2500 rpm) was conducted for 0.5, 2, 4, 8, 16, 24 h and one sample without stirring was evaluated. After 24 h of incubation time, the supernatant was removed from each well, 100 μL of MTT solution (0.25 mg/mL) was added, 3 h later the supernatant was removed, and then 200 μL of DMSO was added to each well. Then the absorbance of each well at 570 nm was determined by using a microplate reader (Infinite M200, TECAN, Switzerland). The tetrazolium ring of MTT will be metabolized into blue formazan crystals by cellular metabolic activity. The amount of formazan crystals produced is proportional to the number of living cells. From the absorbance value of formazan crystals, the cell survival rate was calculated. The assessment of the cell viability rate of amyloid-like oligomers was conducted on N2a cells with different incubation times and different concentrations. Similarly, the cytotoxicity assessment of oAβ_{42} with different concentrations (0, 5, 10, 15, 20, 25, 30, 40 and 50 μM) was evaluated.

2.8. Cellular uptake of oAβ_{42} by N2a cells with and without SPION stirring treatment

The cellular uptake studies of oAβ_{42} with and without SPION stirring treatment were conducted with N2a cells. The N2a cells (2×10^5 cells/well) were cultured in DMEM (high glucose, 1 % FBS, without phenol red) medium in a 6-well cell culture plate for 24 h. The experimental groups were prepared as follows: (1) Control; (2) oAβ_{42} (25 μM); (3) oAβ_{42} (25 μM) + SPIONs (200 μg/mL); (4) oAβ_{42} (25 μM) + SPIONs (200 μg/mL) with stirring; (5) SPIONs (200 μg/mL); (6) SPIONs (200 μg/mL) with stirring. Cells without any treatment served as the control group. The treatment groups with stirring were placed on an electromagnetic stirrer and stirred at 2500 rpm for 30 min at 37 °C. After 24 h of co-incubation, the cells were washed with PBS thrice, and fixed with 4 % formaldehyde. Then the wells were washed with PBS three times, and 0.1 % Triton X-100 was added to increase cell permeability. To detect the formation of Aβ species with a β structure, ThT (50 μM) was used for staining. The staining was conducted in conditions for 1h at RT. After washing thrice with PBS, the cell nuclei were stained with Hoechst 33342 (5 μg/mL) for 15 min. Then they were washed thrice with PBS and finally, the cells were fixed on a glass slide with an 18 μL mounting medium. Confocal laser scanning microscopy (ZEISS, LSA-780) was used to observe the fluorescence of each group. The excitation wavelengths used were 405 nm (Hoechst) and 458 nm (ThT). Calculation of the fluorescence intensity was done using Image-Pro Plus 6.0 software.

2.9. Morphology and cellular functions of N2a cells treated with oAβ_{42} and SPION stirring

The effect of magnetic stirring treatment on N2a cells co-cultured with oAβ_{42} was assessed. The N2a cells (2×10^5 cells/well) were cultured in DMEM (high glucose, 1 % FBS, without phenol red) medium in a 6-well cell culture plate for 24 h. The cells were then treated with

the experimental groups as discussed in the previous experiments. After 24 h of co-incubation, the cells were washed with PBS thrice, and fixed with 4 % formaldehyde. Then the wells were washed with PBS three times, and 0.1 % Triton X-100 was added to increase cell permeability. The F-actin staining kit was used to stain the cytoskeleton of the cells according to the manufacturer's instructions. The cells were incubated for 30 min, then removed, and washed with PBS thrice. The nucleus of the cells was stained by Hoechst 33342 as described in previous experiments. Then, the coverslip was taken from the well and mounted over a glass slide, sealed with nail polish, and used for imaging. A confocal microscope was used to observe the fluorescence signal. The excitation wavelengths used were 405 nm (Hoechst) and 488 nm (F-actin) respectively. Similarly, the cellular functions of specific protein expressions were evaluated using laser scanning confocal microscopy (LSCM). The treatment groups with stirring were placed on an electromagnetic stirrer and stirred at 2500 rpm for 30 min at 37 °C. After treatment, the co-incubated cells were washed with PBS three times and fixed with 4 % formaldehyde. After fixation (ca 15 min), the solution was removed and washed with PBS. 0.1 % Triton X-100 and blocking buffer was added to increase the cell permeability and prevents non-specific binding; later, the solution was removed and washed thrice with PBS. Then the cells were co-incubated with either one of the primary antibodies for 24 h at 4 °C (chicken anti-MAP2 antibody (1:200) or Mouse anti-beta III Tubulin antibody (1:200), or rabbit anti-caspase 3 (1:200)). The primary antibody was removed after 24 h, washed with PBS three times, and then the cells were incubated with corresponding secondary antibody for 1 h at room temperature. Followed by washing three times with PBS. Further, the F-actin staining kit was used to stain the cytoskeleton of the cells, and Hoechst 33342 solution (5 μg/mL) was used to stain the cell nuclei. Finally, the coverslips were washed, placed on the 40 μL mounting medium, and then fixed on a glass slide. The ROS generation by N2a cells was evaluated by co-incubating N2a cells with different experimental groups with and without stirring. Later, the medium was removed and the cells were washed and fixed with 4 % formaldehyde. Then Hoechst 33342 solution (5 μg/mL) was used to stain the nucleus. LSCM was used to observe the fluorescence signals from each group. The fluorescence signals from each group were analyzed using LSCM. The excitation wavelengths of the laser light used were 405 nm (Hoechst), 488 nm (F-actin), and 633 nm (Alexa Fluor® 647), 488 nm (DCF-DA), respectively, and the subsequent fluorescence quantification was done with Image-Pro Plus 6.0 software. For flow cytometric analysis, N2a cells were seeded in 6-well plates. After 24 h, the cells were treated as different groups as aforementioned, washed with PBS, trypsinized and harvested. The harvested cells were subjected to live/dead staining with Annexin V/PI for viability measurement by flow cytometry (BD Biosciences instruments). For ROS staining, DCF-DA (25 μM) was used. For the MAP2 and β3-tubulin measurements, the cells were immunofluorescence (IF) stained with the MAP2 and β3-tubulin markers and the intracellular fluorescence intensity was determined by flow cytometry.

2.10. Cytokine release from BV-2 cells treated with oAβ_{42} and SPION stirring and the impact of released cytokines on N2a cells

The cytokines released by the BV-2 cells incubating with oAβ_{42} and the change in cytokine production under magnetic stirring with SPIONs were evaluated. The BV-2 cells (1.2×10^5 cells/well) were cultured in 24 well plates for 24 h with DMEM (High glucose, 10 % FBS, without phenol red). After 24 h the cells were treated with the experimental groups as described in the previous experiment. The treatment groups with stirring were placed on an electromagnetic stirrer and stirred at 2500 rpm for 30 min at 37 °C. After the stirring treatment, the cells were re-incubated for 36 h, and then the supernatant of each group was taken. An ELISA assay kit was used to evaluate the difference in cytokine production (IL-6, TNF-α, IL-10) in the cell supernatant. To evaluate the impact of cytokines released by macrophages on N2a cell survival rate, the culture medium from different treatment group with BV-2 cells was transferred to N2a cells (1.5×10^4 cells/well) cultured in 96-well plates for 24 h. Later, the survival rate of N2a cells in each group was subsequently analyzed using the MTT assay.

2.11. Cellular uptake of mpAβ by BV-2 cells

Microglial cells (BV-2 cells, 1.8×10^5 cells/well) were cultured using DMEM (High glucose, 10 % FBS, without phenol red) in a 6-well cell culture plate for 24 h. The cells were co-incubated with different treatment groups for 24 h. The BV-2 cells without any treatment were considered as a control group. After 24 h of co-incubation, the cells were washed with PBS three times, then 4 % formaldehyde was added to fix the cells. After fixation, 0.1 % Triton X-100 was added to increase cell permeability. Later, the cells were incubated with ThT (50 μM) in dark conditions at room temperature for 1 h. The cells were washed with PBS three times and stained with Hoechst 33342 (5 μg/mL) for the cell nuclei. LSCM was used to observe the fluorescence signals from each group. The excitation wavelengths of the laser light used were 405 nm (Hoechst), and 458 nm (ThT), respectively, and the fluorescence value was analyzed by the Image Pro Plus 6.0 software.

2.12. Experimental animals and treatments

The male C57BL/6 mice (4–5 weeks old) were used for all experiments and were purchased from the National Laboratory Animal Center, Taiwan. Approved guidelines for the care and use of laboratory animals from the Institutional Animal Care and Use Committee (approved number for animal use; IACUC 110024) were followed throughout the study. The mice were kept under controlled temperature (24 °C ± 1 °C), humidity (50%–60 %), and a light/dark cycle of 12/12 h. A standard rodent diet and water were supplied to all the animals. To obtain an AD mouse model with early oAβ_{42} deposition, the six-week-old mice were injected with 3 μL of oAβ_{42} (40 μM) into the right hippocampus region of the brain (anteroposterior, 2.0 mm; mediolateral, 1.3 mm; dorsoventral 2.2 mm) using a stereotaxic instrument and a 27G needle. All the mice experiments have the following six groups. The experimental groups were prepared as follows: (1) Healthy control group; (2) Injected with 3 μL of PBS solution (25 μM); (3) Injected with oAβ_{42} (40 μM) (4) oAβ_{42} (40 μM) + SPIONs (200 μg/mL) (5) oAβ_{42} (40 μM) + SPIONs (200 μg/mL) + stirring; (6) SPIONs (200 μg/mL) with stirring. Mouse without any treatment served as the control group. The treatment groups with stirring were placed on an electromagnetic stirrer and stirred at 2500 rpm for 30 min at RT.

2.13. Nest construction experiment

Nesting experiments were conducted to test the characteristics of rodents instinctively collecting materials for building nests. The results of this experiment were used to evaluate the behavioral changes induced by Aβ species in mice. The mice were separated into six groups as explained above, and the investigations were started after two weeks of the injections. Each group had five mice for the experiment. Each mouse was placed in a cage with five pieces of paper (paper size 10 cm * 7 cm). Then the quality of the nest constructed by the mouse was evaluated for the next five days. For further confirmation, the same test was conducted with the help of cotton lint (5 cm* 5 cm * 0.5 cm), and the results were evaluated.

2.14. Barnes maze study

The Barnes maze is used to test the memory of animals, which is mainly designed using the characteristics of rodents, that is, their response to light (preference towards darkness). The Barnes maze apparatus consists of multiple holes (20 numbers) with a 5 cm diameter on the circular platform (100 cm diameter) with four quadrants. In the

left quadrant, one hole was arranged to be dark and was assigned as the target hole for the mice. The mice were trained to remember the dark hole to hide. The movement of mice through the maze was recorded using a camera (MB AHD34HP) to count the relevant values. Then, the data was evaluated by RVTR software. Briefly, a Barnes maze with 20 holes where one hole was set as a hiding place for mice without light was used. A fluorescent lamp 240 cm above the maze was used as a light source. Before training, the mice were starved for 8 h, and feed was placed in the hiding hole to strengthen the motivation of the mice to move towards the hole. Trained 3 times a day, with at least 1 h interval between each training session, and each training time was not exceeded by 3 min for 5 days. The mice were used for an experiment two weeks after injection. On the sixth day, the holes in the hiding place were closed and the mice were placed in the middle of the maze, then the movement and retention of the mouse were evaluated to check whether the mice had normal memory or not. The mice moved to the closed hole or the left quadrant were considered as healthy. The mice moved to other holes and waited in other quadrants, which was considered as memory loss. The experimental groups were assigned similarly to the above experiment.

2.15. Animal sacrifice, tissue embedding and tissue sectioning

The mice were euthanized using carbon dioxide. The brains of the mice were collected, washed and were placed in an embedding box. Followed by embedding the brain with an optimal cutting temperature compound (OCT (4538, SAKURA, USA)), and finally placed in a −80 °C refrigerator. Prior to tissue sectioning, the embedded boxes were moved to −20 °C. Tissues were sliced using a microtome to 10 μm size and placed on a glass slide and finally stored in a refrigerator at −20 °C. Tissue staining was further done to evaluate the performance of SPIONs in neurotoxicity alleviation and elimination of oAβ_{42} from the brain of mice.

2.16. Brain tissue imaging

Three tissues from each treatment group were selected for the experiment. After removing the OCT and rehydrating the tissues, the slides were dipped in haematoxylin as mentioned above. Then the tissues were soaked in DIW for 1 min. The tissues were subsequently immersed in solution-I, composed of ethanol (80 %) and excess NaCl, followed by mixing with a 1 % v/v NaOH solution, and left to incubate for 30 min in darkness at RT. Afterwards, the tissues were transferred to CR solution, with a final concentration of 0.2 % w/v, and mixed with a 1 % NaOH solution, then allowed to stand for 20 min in darkness at RT. Later, the tissues were dipped in ethanol (99 %) for 5 s and in xylene for 10 s to complete the dying process. For Nissl staining After removing OCT from the tissues, they were immersed in cresyl purple solution containing cresyl violet acetate (0.2 % w/v) and acetic acid (0.3 % v/v) in deionized water (DIW), then placed in darkness at 40 °C for 20 min. Subsequently, the tissues were briefly soaked in DI water for 10 s, followed by a 10 s immersion in 70 % ethanol and a 3 min soaking in xylene. For the Prussian blue staining The OCT free tissues were dipped in a solution made by mixing potassium ferrocyanide (10 % w/v) and hydrochloric acid (20 % v/v) in 1:1 ratio, and allowed to stand at RT for 20 min. Followed by Soaking the tissues in DI water for 1 min at RT. Then the tissues were dipped in the nuclear fast red solution (Nuclear fast red, 0.1 % w/v) and allowed to stand for 3 min at RT. After the procedure, the tissues were soaked in ethanol (95 %) for 10 s at RT. For H & E staining, the tissues were soaked in haematoxylin solution, for 1 min at RT, and rinsed with tap water, then the tissues were dipped in ammonia solution (0.25 %) for 10 s at RT and rinsed with tap water. After rinsing, the tissues were dipped in eosin solution for 1 min at RT, and later rinsed with ethanol (95 %). For IHC staining the primary antibodies used in this experiment were rabbit anti-beta amyloid antibody (1:200), rabbit anti-caspase 3 (1:200), rabbit anti IBA1 (1:200), rabbit anti-CD68 (1:200), mouse anti-GFAP (1:200), rabbit anti-EAAT2 (1:200), chicken anti-MBP (1:200). The secondary antibodies used were goat anti-rabbit alexa fluor 488 (1:200), goat anti rabbit FITC (1:200), goat anti-mouse FITC (1:200), goat anti-chicken FITC (1:200). Followed by staining, the slides were imaged using an upright fluorescent microscope.

2.17. Animal body weight

The body weight of mice was recorded every 3 days from the day of injection to the day of the sacrifice to roughly evaluate the health of the mice.

2.18. Statistics

The data processing of this study used the student t-test in Excel to analyse the data by an unpaired two-tailed *t*-test and one-way ANOVA with Bonferroni multiple comparisons. Statistical significance is indicated as (n.s.) $P > 0.05$, (*) $P < 0.05$, (**) $P < 0.005$ and (***) $P < 0.001$. When p-value <0.05, it was regarded as a significant difference.

3. Results and discussion

3.1. Synthesis and characterization of OA-SPIONs and SPIONs

In this study, a new therapeutic strategy featuring the absence of conventional drugs and the accompanied side effects was proposed. SPIONs were prepared to serve as magnetic nanospinners for capturing and eliminating oAβ_{42} species from brain tissue under rotating magnetic field for the AD treatment. To attain the magnetic nanospinners, OA-SPIONs were first prepared by thermal decomposition technique and were further exchanged with citric acid by ligand exchange reaction to get CA-SPIONs being further referred to as SPIONs in this work. Replacing OA with CA on OA-SPIONs improves their aqueous colloidal dispersion. The OA-SPIONs and SPIONs were characterized by TEM, SEM, DLS, XRD, SQUID, TGA. The results are shown in Fig. S1 and Fig. S2 respectively**.** The TEM images of SPIONs showed the mean size of ca 20 nm, similar to the nanoparticles without citric acid coating. With the nanoparticles being spherical in morphology, the tissue/cell damage caused by the SPIONs magnetic stirring treatment for accreting oAβ_{42} species into magnetic plaques can be minimized both in vivo and in vitro. The DLS characterization showed the Dh of the nanoparticles around 40.40 ± 5.54 nm in DIW (Table S1, Fig. S2c). The increase in Dh is ascribed to the hydrated citric acid layers over the SPION surfaces. The zeta potential measurement (Table S1) indicates a negative value of ca −21.9 mV, confirming the presence of citric acid on the particle surfaces. The presence of negatively charged carboxylate groups over the surface of SPIONs not only improves the colloidal stability in aqueous phase via electrostatic repulsion, but also helps develop interactions with amyloid species. The XRD examination of OA-SPIONs indicates diffraction peaks (Fig. S1e to Fig. S1d) in consistence with the profile of Fe_3O_4 (JCPDS card number 82–1533) [35], being indexed to the characteristic cubic unit cell of the magnetite phase. The magnetization saturation (emu/g) of SPIONs as a function of the applied magnetic field (Oe) showed that the nanoparticles exhibit a superparamagnetic behaviour and a magnetic saturation of ca 60 emu g-1. The magnetic behaviour was reversible at 300 K. No hysteresis, neither coercivity nor remanence, was observed. The TGA data illustrated, respectively, in Figs. S1f and S2e indicate that the Fe content was ca 91 % for OA-SPIONs before the citric acid coating and 80 % for SPIONs. The colloidal stability of the nanospinners in aqueous phase was evaluated in terms of the change in light scattering intensity from the DLS measurements of SPIONs with the concentrations up to 200 μg/mL in DIW, PBS, and DMEM, respectively. As shown in Fig. S3, the SPIONs exhibit good dispersion with negligible variation in light scattering intensity in different aqueous solutions over a time period of 120 min at 37 °C.

3.2. Accretion of oAβ_{42} by SPION stirring

The stirring effect of SPIONs under rotating magnetic field is seen by the accelerated diffusion of highly water-soluble CR dye in water (Fig. S4). CR is an azo dye, yielding a red-colored solution when being thoroughly mixed with water. A small drop of aqueous CR solution (20 μL) was carefully added into a water droplet in the absence and presence of SPIONs under an external magnetic field. Without magnetic stirring, the dye species resided locally at a spot within the water droplet. However, the dye species subjected to magnetic stirring at 2500 rpm with SPIONs became rapidly distributed within the droplet, the extent of dispersion being dependent on the stirring duration. Notably, a homogeneous aqueous solution of CR was achieved over 60 s of stirring at 2500 rpm. Owing to the good aqueous dispersion colloidal stability, the SPIONs were thoroughly dispersed in the aqueous droplet, leading to homogenous and effective stirring in the local droplet under the magnetic field treatment. It has been reported previously that magneto-mechanical force induced by magnetic nano/micro particles under a magnetic field led to cell ablation [26,27]. It is thus necessary to evaluate the cellular ablation effect of SPIONs with stirring. The survival data of N2a cells treated with magnetic stirring of SPIONs of various concentrations by the MTT assay are shown in Fig. S5a. No significant change in cell survival rate was observed with the cells receiving the stirring treatment within 4 h in the SPIONs concentration range employed up to 200 μg/mL. The cell viability of N2a cells after the SPION stirring treatment was also evaluated by Annexin V/PI staining with flow cytometric measurement. As shown in Fig. S5b, the cell viability remains high (about 80 %) with SPION stirring treatment at the SPION concentration of 200 mg/mL and the stirring speed of 2500 rpm up to 4 h.

With the observed stirring effect of SPIONs under a magnetic field alongside the excellent cellular survival (Figs. S4 and S5), the ability of the SPIONs via stirring to accrete cohesive oAβ_{42} species into large aggregates was evaluated. The preparation and characterization of oAβ species were conducted according to the methods described previously [33,34]. Aggregation of Aβ_{42} species into oAβ_{42}, Aβ fibrils and naturally occurring Aβ plaques (referred to as npAβ hereinafter to distinguish from magnetic Aβ plaques) in aqueous Aβ solutions was demonstrated by ThT fluorescence measurements, dot blot method, TEM, and AFM-SPM. ThT is a frequently used probe to identify mature amyloid fibril formation. The benzylamine and benzathiole rings of the ThT dye bind to the β-sheet structure of various Aβ aggregates, especially in fibril, or plaque structures [36]. The fluorescence intensity of ThT in the aqueous oAβ_{42} solution with the time-evolved formation of naturally occurring plaques for 5 days were evaluated. As seen in Fig. 2a, the ThT fluorescence intensity was rather low with the onset of the incubation and increased significantly over 20 h. The increase in fluorescence intensity is ascribed to the increasing binding of benzylamine and benzathiole rings on ThT dye to the abundant β-sheet structure on the Aβ aggregates (including oligomers, fibrils and npAβ) formed during the pre-incubation. From the data, it is evident that Aβ peptides oligomerized to oAβ42 within 20 h. The fluorescence intensity reached a plateau since then over 120 h incubation, indicating the formation of Aβ species into matured fibrils and npAβ, which are not distinguishable by ThT. The dot blot assay of an amyloid-like model was further used to detect the time required to form Aβ_{42} oligomers and fibrils by adopting the antibodies to identify separately the oligomers and the fibrils over various incubation time intervals. The data are shown in Fig. 2b. Obviously, the strongest signal

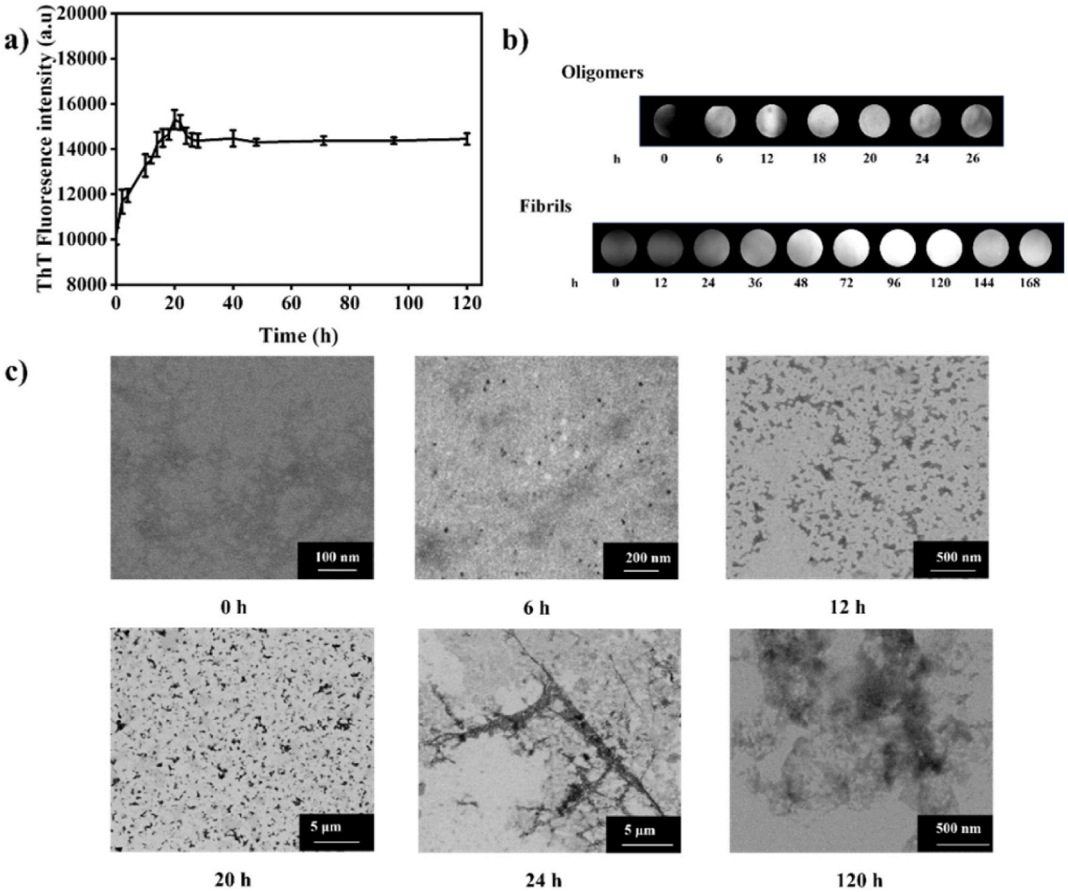

Fig. 2. (a) ThT fluorescence intensity of Aβ_{42} (20 μM) in PBS with different incubation times. (b) Dot blot analysis of the formation of Aβ_{42} oligomers and fibrils using anti-oligomer and anti-fibril antibodies with different incubation times. (c) TEM images of various Aβ_{42} species (50 μM) after incubation in PBS at 37 °C for different times.

intensity signifying the oAβ_{42} formation appeared at the incubation time of 18–20 h while the specific anti-fibril antibody showed signal increases after 24 h incubation, indicating the formation of fibrils or naturally occurring plaques. TEM and AFM were also employed to determine the time-evolved aggregate structures of Aβ_{42} along with the incubation reaction. The TEM images shown in Fig. 2c illustrate the size of the Aβ species below 20 nm after 6-h incubation. With being incubated over 20 h, the formation of oAβ_{42} or soluble protofibrils with the sizes around 100–200 nm was observed, indicating presumably the formation of Aβ fibrils, in consistence with the data attained from the dot blot assay (Fig. 2b). Upon further incubation over 120 h, the TEM image showed a cloudy structure of Aβ, suggesting the transformation of Aβ species into naturally occurring plaques. From the AFM data, little change in the conformation of Aβ species was observed within 6 h of incubation (Fig. S6). The small Aβ species under examination was no more than 10 nm in height. In contrast, the Aβ species obviously underwent agglomeration into oAβ_{42} with a size of ca 100–200 nm in width, and 50 nm in height with the incubation exceeding 20 h. After incubation for 72 or 120 h, abrupt increases in size of the Aβ aggregates to the micrometer range were observed, indicating the formation of the Aβ plaques. With all the data attained from TEM, AFM, ThT, and dot blot assay, it is rather evident that the Aβ_{42} monomers are transformed into oAβ_{42} with 20 h incubation and the mature fibrils form rapidly over 24 h, followed by the plaque formation with incubation being further proceeded over 72 h.

The magnetic stirring effect of SPIONs on altering oAβ_{42} structure was evaluated at a stirring speed of 2500 rpm with various concentrations of the nanospinners in aqueous phase. The fluorescence intensity measurements of CR and ThT and the AFM examination were adopted separately to evaluate the accretion of oAβ_{42} caused by the SPIONs magnetic stirring. As shown in Fig. 3a, the fluorescence intensities of both ThT and CR were found to increase with the oAβ_{42} solution receiving the SPION stirring treatment compared to the oAβ_{42} only and oAβ_{42}+SPIONs groups without stirring treatment. The enhancement in the fluorescence intensity is ascribed to the formation of mpAβ. Fig. 3a also shows the increase of the fluorescent intensity of ThT and CR with the increase of the concentration of SPIONs (0 < 100 < 200 μg/mL) employed under magnetic rotating field, confirming the agitation by the nanospinners to induce the agglomeration of oAβ_{42}. AFM was employed to further corroborate the capture and accretion of oAβ_{42} by magnetic stirring. Both the 2-D and 3-D AFM topographic maps verify the mpAβ formation induced by the SPION stirring (Fig. 3b). With the SPION stirring treatment, the AFM height profile shows that SPIONs-enclosed Aβ aggregates, termed as mpAβ, are more than 50 nm in height while the dimension of the base area of the plaque reached micrometer scale. By contrast, oAβ_{42} without stirring remained less than 50 nm in height and 200 nm in the dimension of the base area. The results clearly demonstrate that the magnetic stirring with SPIONs exhibits the capability to remove oAβ_{42} species in aqua by agglutination together into mpAβ. In addition to the inherent cohesive property of oAβ_{42} to form plaques, there are two possible mechanisms involved for SPION stirring to accelerate the accretion of small oAβ_{42} species into plaques. First, the stirring treatment can obviously increase the contact of the oAβ_{42} species, which is a required step to initiate plaque formation. Second, the rotational magnetic field causes the SPIONs to spin, generating a centripetal force that moves the surrounding fluid containing oAβ_{42} toward the SPIONs, facilitating their aggregation into mpAβ.

3.3. *Effects of oAβ_{42} and mpAβ on N2a neural cells*

Prior to studying the accretion effect of oAβ_{42} into mpAβ in vitro, the cell viability of N2a cells treated with Aβ_{42} (25 μM) pre-incubated for different time intervals was evaluated. The results are shown in Fig. 4a. As expected, the cell survival rate evaluated by the MTT assay was appreciably decreased when being treated with Aβ_{42} preincubated for 20 h. The cell viability was then gradually increased to 90 % with Aβ_{42} being pretreated for 120 h. In consistence with the previous data, the onset of the formation of oAβ_{42} by preincubation occurs approximately at 20 h at which the lowest cell viability was observed among different aggregates of Aβ_{42}. This signifies the enhanced cytotoxicity of oAβ_{42} compared to other Aβ species (Fig. 4a) in agreement with the observations reported elsewhere [37]. Fig. 4b also indicates that the cytotoxicity of oAβ_{42} toward N2a cells increases with the concentration of the oAβ_{42}

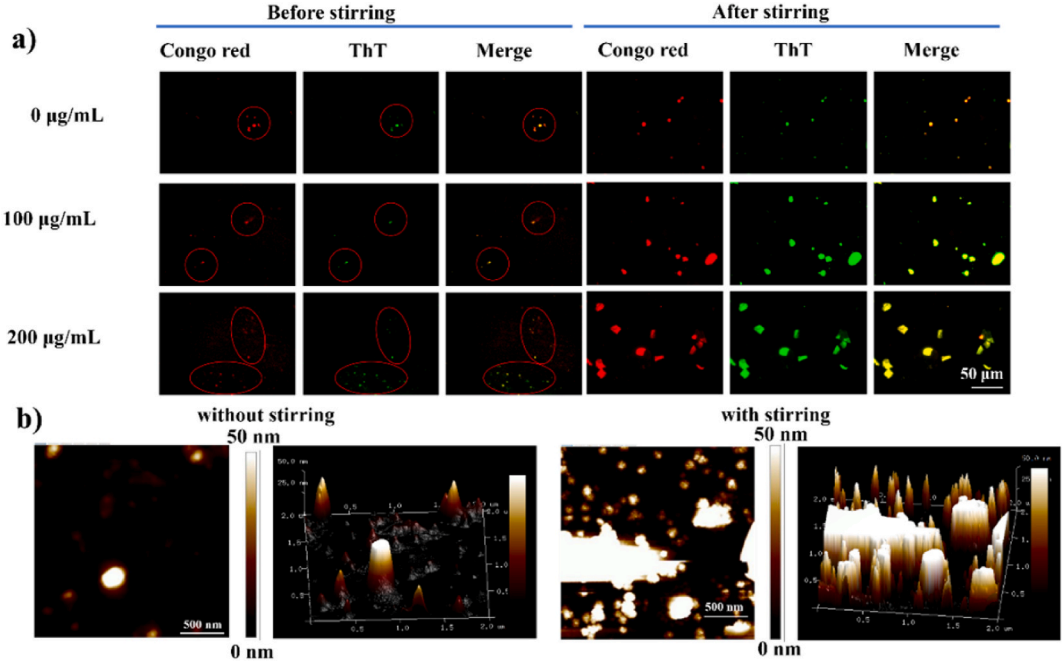

Fig. 3. (a) Fluorescence images of accretion of oAβ_{42} (25 μM) by SPIONs stirring treatment with different SPIONs concentrations (0, 100 and 200 μg/mL) at 2500 rpm for 30 min. The Aβ species were stained with CR (red) and ThT (green), respectively. (b) AFM 2-D and 3-D images of oAβ_{42} (25 μM) with and without the SPIONs (200 μg/mL) stirring treatment at 2500 rpm for 30 min. (For interpretation of the references to color in this figure legend, the reader is referred to the Web version of this article.)

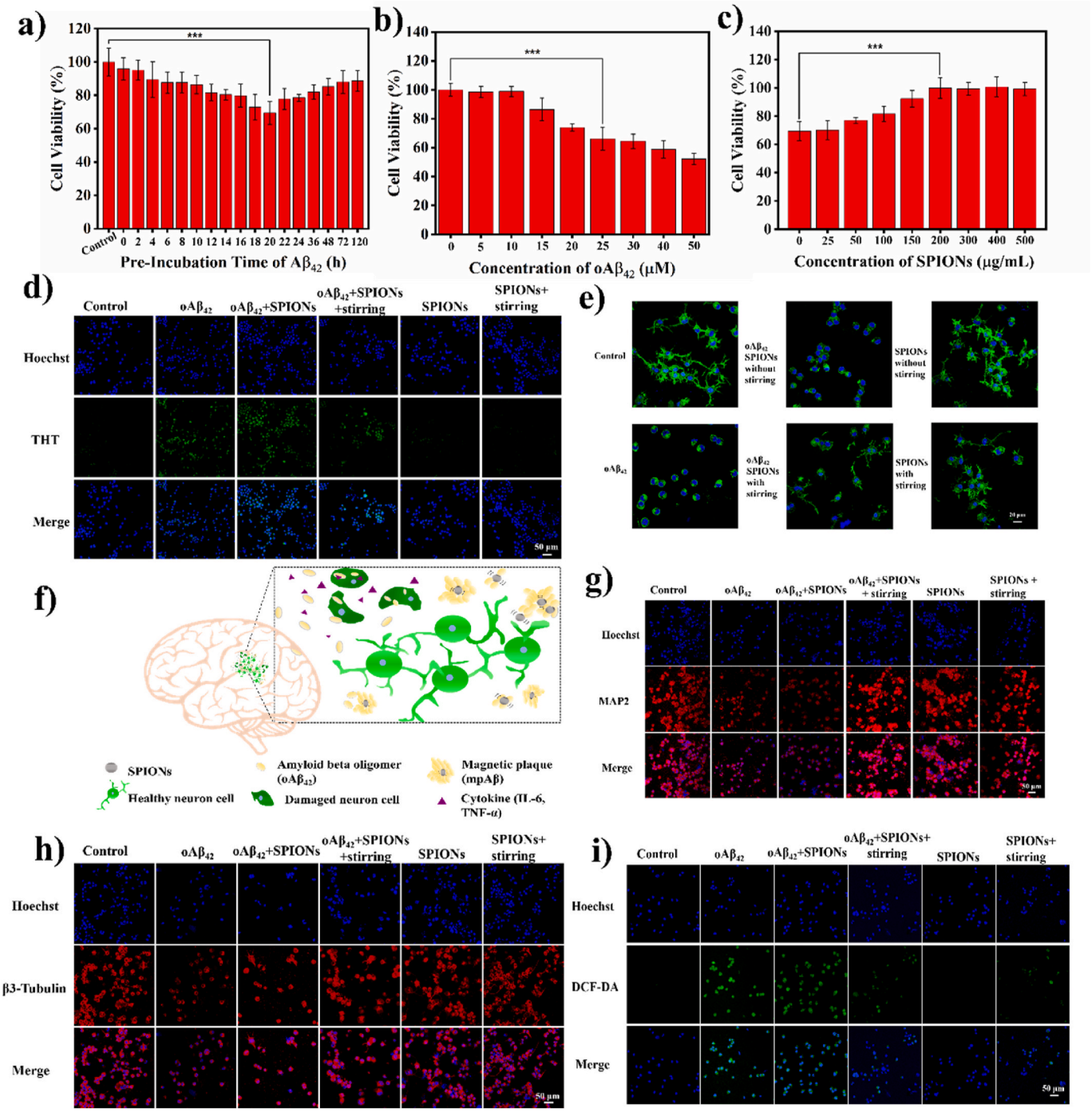

Fig. 4. (a) Cell viability of N2a cells after 24 h incubation with $A\beta_{42}$ (25 μM) pre-treated over different time intervals. The cell viability was determined by the MTT assay. (b) Cell viability of N2a cells after the incubation with $oA\beta_{42}$ of varying concentrations for 24 h. The $oA\beta_{42}$ was attained by preincubation of $A\beta_{42}$ in PBS for 20 h. (c) Cell viability of N2a cells treated together with $oA\beta_{42}$ (25 μM) and SPION magnetic stirring with different SPION concentrations at 2500 rpm for 30 min. (d) LSCM images of N2a cells incubated with $oA\beta_{42}$ (25 μM) and SPIONs (200 μg/mL) without and with magnetic stirring at 2500 rpm for 30 min to evaluate the cellular uptake of $oA\beta_{42}$. Cell nuclei (blue) and $oA\beta_{42}$ (green) were stained with Hoechst and ThT, respectively. Scale bar 50 μm. (e) Morphology of N2a cells receiving various treatments. Scale bar 20 μm. (f) Graphical representation of the SPION stirring treatment safeguarding the neuronal cells from the uptake of $oA\beta_{42}$. (g) Images of N2a cells receiving various treatments highlighting the intracellular MAP2 fluorescence signals (in red). Scale bar 50 μm. (h) Images of N2a cells receiving various treatments highlighting the intracellular β3-tubulin fluorescence signals (in red). Scale bar 50 μm. (i) Fluorescence images of intracellular ROS stained with DCF-DA in N2a cells receiving various treatments. Scale bar 50 μm. (For interpretation of the references to color in this figure legend, the reader is referred to the Web version of this article.)

once beyond 10 μM. The cell viability was reduced to around 58 % at the $oA\beta_{42}$ concentration of 50 μM. The effect of the SPION stirring treatment on $oA\beta_{42}$-induced cytotoxicity against N2a cells was evaluated with the agitation time of 30 min and the stirring speed 2500 rpm. Fig. 4c shows the cell viability of N2a cells treated with 20 h pre-incubated $A\beta_{42}$ (25 μM), followed by 30 min magnetic stirring treatment as a function of the SPION concentration. While the cell viability of N2a cells without stirring treatment shows significant reduction, the reduction in cell viability

of N2a cells caused by the pre-incubation of $A\beta_{42}$ is alleviated with the SPION magnetic stirring. A strong dependence of the cell viability on the SPION concentration adopted for magnetic stirring under rotating magnetic field was observed. The cytotoxicity of $A\beta_{42}$ species against N2a cells even after 20 h pre-incubation was highly reduced to an undetectable extent by the magnetic stirring treatment at the SPION concentration of 200 μg/mL or beyond. The data clearly demonstrate the capability of the SPION magnetic stirring to eliminate the $oA\beta_{42}$ cytotoxicity by accreting them into mpAβ, rendering the neurons highly viable.

It has been reported that the intraneuronal accumulation of $oA\beta_{42}$ species is a key factor to induce its cytotoxicity against neurons [34]. Fig. 4d shows the uptake of $oA\beta_{42}$ by N2a cells with and without SPION stirring treatment using ThT as a fluorescence probe to label the β sheets of the $A\beta_{42}$ aggregates. The N2a cells receiving the $oA\beta_{42}$+SPIONs+-stirring treatment exhibited much reduced intracellular ThT fluorescence intensity compared to both the $oA\beta_{42}$ group and the $oA\beta_{42}$+SPIONs without stirring group. This indicates that the cellular uptake of the $oA\beta_{42}$ species or the aggregates produced by the SPION stirring treatment was reduced, most probably because of the formation of mpAβ which are too large in size to be internalized by neuron cells. Fig. 4e shows the morphology of the N2a cells subjected to various treatments, including the $oA\beta_{42}$ group and the $oA\beta_{42}$+SPION+stirring group. With being treated with either $oA\beta_{42}$ alone or $oA\beta_{42}$+SPIONs in the absence of stirring, the N2a cells exhibited their neurites (axons and dendrites) appreciably shorter compared to the blank control group. By contrast, the neurite length was largely retained in the $oA\beta_{42}$+-SPION+stirring group. The cytotoxicity caused by $oA\beta_{42}$ toward the neuron cells in terms of the cell integrity was obviously alleviated by the SPION stirring treatment that captured the Aβ oligomer species into large aggregates. A graphical illustration of SPION stirring treatment safeguarding the N2a cells from the uptake of $oA\beta_{42}$ is shown in Fig. 4f. The mitigation of the cell functional impairment induced by $oA\beta_{42}$ with the SPION stirring treatment was also evaluated in terms of related cellular protein expression. Microtubule-associated protein-2 (MAP2) and class III β-tubulin (β3-tubulin) were chosen as the markers. Comparisons among the blank control and various treatment groups on neuron-specific protein expression of cells were illustrated in Fig. 4g and h. The quantified data based upon the normalized fluorescence intensity to the blank control group are shown in Figs. S7a and S7b. Both the MAP2 and β3-tubulin protein expression was significantly suppressed with the $oA\beta_{42}$ groups in the absence of SPION stirring treatment. The reduction is mainly ascribed to the toxic action of $oA\beta_{42}$ on the neuron cells. With the N2a cells receiving the SPION stirring treatment in the absence of $oA\beta_{42}$, the expression of MAP2 and β3-tubulin protein remains essentially identical to the control group, indicating normal cellular functions of the treated cells with the SPION stirring treatment. More importantly, the $oA\beta_{42}$+SPIONs+stirring group shows the relatively high protein expression by the fluorescence staining, the extent being comparable to the control group. The fluorescence staining of MAP2 and β3-tubulin in N2a cells receiving various treatments was also examined by flow cytometry. Similar observations showing comparable MAP2 and β3-tubulin expression between the control and $oA\beta_{42}$+-SPIONs+stirring group and appreciable reductions in the two protein levels in the $oA\beta_{42}$ group without stirring treatment were observed in Fig. S7c (MAP2) and **S7d** (β3-tubulin), respectively. This consistency in the fluorescence intensity corroborates the efficacy of the SPION stirring in protecting the cells from $oA\beta_{42}$ induced cellular damage by agglomerate $oA\beta_{42}$ species into large plaques. Excessive free radical (ROS) generation is the key event causing progressive neuronal damage in AD. Multiple studies have shown that $oA\beta_{42}$ induces brain oxidative stress [38–40], resulting in the generation of ROS. To validate this finding, the variation of ROS level induced by $oA\beta_{42}$ inside N2a cells was evaluated. The fluorescence images of intracellular ROS stained with DCF-DA in the N2a cells receiving various treatments are shown in Fig. 4i. The quantified fluorescence intensity data are illustrated in Fig. S7e. Similar observation was attained by the measurements of intracellular ROS (DCF-DA) fluorescence intensity of N2a cells with various treatments by flow cytometry. The data are shown in Fig. S7f. While the control group representing the N2a cells in the absence of treatment exhibits the lowest fluorescence intensity among all groups, the N2a cells treated with only $oA\beta_{42}$ show appreciably enhanced DCF-DA fluorescence signal, thereby confirming the $oA\beta_{42}$-mediated ROS generation. Since it is very often that the reactive species is generated by reactive metal nanoparticles triggering a cascade of intracellular reactions following their cellular uptake [41], the ROS generation by SPIONs and SPIONs+stirring was evaluated. The data illustrate that the reactive radical species generated by the incubation of N2a cells with SPIONs were barely detected. The magnetic stirring with SPIONs somewhat enhances the fluorescence intensity of DCF-DA in the cells, indicating the elevation of intracellular oxidative stress caused by the stirring treatment. To get a better insight into the intracellular ROS generation by SPION stirring, the time-evolved DCF-DA fluorescence intensity was evaluated. The results as shown in Fig. S7g indicate the slight increase in the oxidative stress with the increase in the treatment duration, in particular, beyond 1 h. This may be ascribed to the accelerated Fenton reaction of bare SPIONs with stirring. Nonetheless, the ROS level generated by $oA\beta_{42}$ is substantially higher in comparison with the SPION stirring. The intracellular ROS level induced by $oA\beta_{42}$ was appreciably reduced with the SPION stirring treatment in large part due to the restriction of the cellular uptake of the stirring-induced agglomerated $A\beta_{42}$ plaques. The observation further signifies the effect of the $oA\beta_{42}$ capture by SPION stirring treatment on preventing cell damages caused by $oA\beta_{42}$-induced oxidative stress in N2a cells. The result also implies that the mpAβ thus formed is not as cytotoxic as $oA\beta_{42}$ and the stirring strategy is efficient to eliminate $oA\beta_{42}$ and prevent its uptake by N2a cells. As aforementioned, the $oA\beta_{42}$ accumulation not only leads to ROS generation but also to neuronal dysfunction and apoptosis. To evaluate the apoptotic effect by $oA\beta_{42}$ accumulation, the level of caspase 3, a lysosomal enzyme involved in the apoptotic pathway, was examined by IHC staining. As shown in Fig. S7h, the caspase fluorescence signal intensity for the SPION group and the SPIONs+stirring group is comparable to the control group, implying that the cellular apoptosis was not additionally promoted by the nanospinners alone or together with stirring treatment. However, the co-incubation of the cells with $oA\beta_{42}$ or $oA\beta_{42}$+SPIONs without stirring showed significantly enhanced signal intensity of caspase 3 compared with the other groups, confirming the inherent cytotoxicity of $oA\beta_{42}$ that induces the increased apoptosis of N2a cells. The data also proved that the capture or accretion of $oA\beta_{42}$ into large plaques by the magnetic stirring of SPIONs reduced their uptake by N2a cells and resulted in the decrease of caspase 3 dependent apoptosis pathway caused by $oA\beta_{42}$.

3.4. *Effects of $oA\beta_{42}$ and mpAβ on BV-2 microglia*

It has been known that activation of microglial cells by the accumulation of oAβ species in brain leads to inflammatory responses that damage neighbouring neuronal cells [38]. To reveal the effects of microglia cell activation by $oA\beta_{42}$ on neuron cells, BV-2 microglial cells were employed in this study serving as the microglial cell model. The response of BV-2 cells to Aβ specie was studied first by the cellular uptake of different Aβ species. As shown in Figs. S8a and S8b, the BV-2 cells treated with $oA\beta_{42}$ only showed weak ThT fluorescence, indicating that the $oA\beta_{42}$ was not efficiently phagocytized by the microglial cells. However, the fluorescence intensity of ThT that stained the β sheet structure of various $A\beta_{42}$ structures was appreciably enhanced with the SPIONs+stirring group, indicating the promoted uptake of Aβ species by SPION stirring treatment. It is evident that the aggregation of $oA\beta_{42}$ induced by the SPION stirring treatment into the magnetic plaque enhances the phagocytic action of BV-2 cells compared to the oAβ species. This is ascribed in part to the enlarged size of the magnetic plaque compared to $oA\beta_{42}$ species. It has been reported previously that the

cellular uptake of fibrillar $A\beta_{42}$ promotes the interactions of CD14 and TLR4 and thus enhances phagocytic activity of microglia through a clathrin-mediated pathway [42]. To further evaluate the actions of microglia with their exposure to various $A\beta_{42}$ species, the cytokines including IL-6, IL-10 and TNF-α, secreted by the microglial cells receiving different treatments were evaluated with ELISA assay. The results are show in Fig. 5a, b and 5c. The production of IL-6 and TNF-α as the pro-inflammatory cytokines was enhanced when the microglia were treated with $oA\beta_{42}$, yet the elevation in proinflammatory cytokine levels was considerably alleviated with the SPION stirring treatment. By contrast, a significant reduction in the anti-inflammatory cytokine, IL-10, with the cells being treated with $oA\beta_{42}$ only was observed. Such a decrease in the IL-10 level was restored with the SPION stirring treatment developed in this work. The uptake of $oA\beta_{42}$ by microglia activates the macrophages in promoting the inflammatory responses, including the increase of pro-inflammatory cytokine secretion and the reduction of the anti-inflammatory cytokines level. With the SPION stirring treatment, the inflammatory response was significantly diminished most probably because of the reduced cellular uptake of $oA\beta_{42}$ as a result of the transformation of the oligomer species into the magnetic plaques. It has been known that macrophages can undergo polarization from M0 to either M1 or M2 phenotype. While the latter is characterized by the anti-inflammatory responses and increased phagocytic capacity, the former is intimately associated with its pro-inflammatory reactions to eliminate the foreign invaders. Therefore, the data shown in Fig. 5a, b and 5c strongly suggest that the $oA\beta_{42}$ uptake induces the polarization of

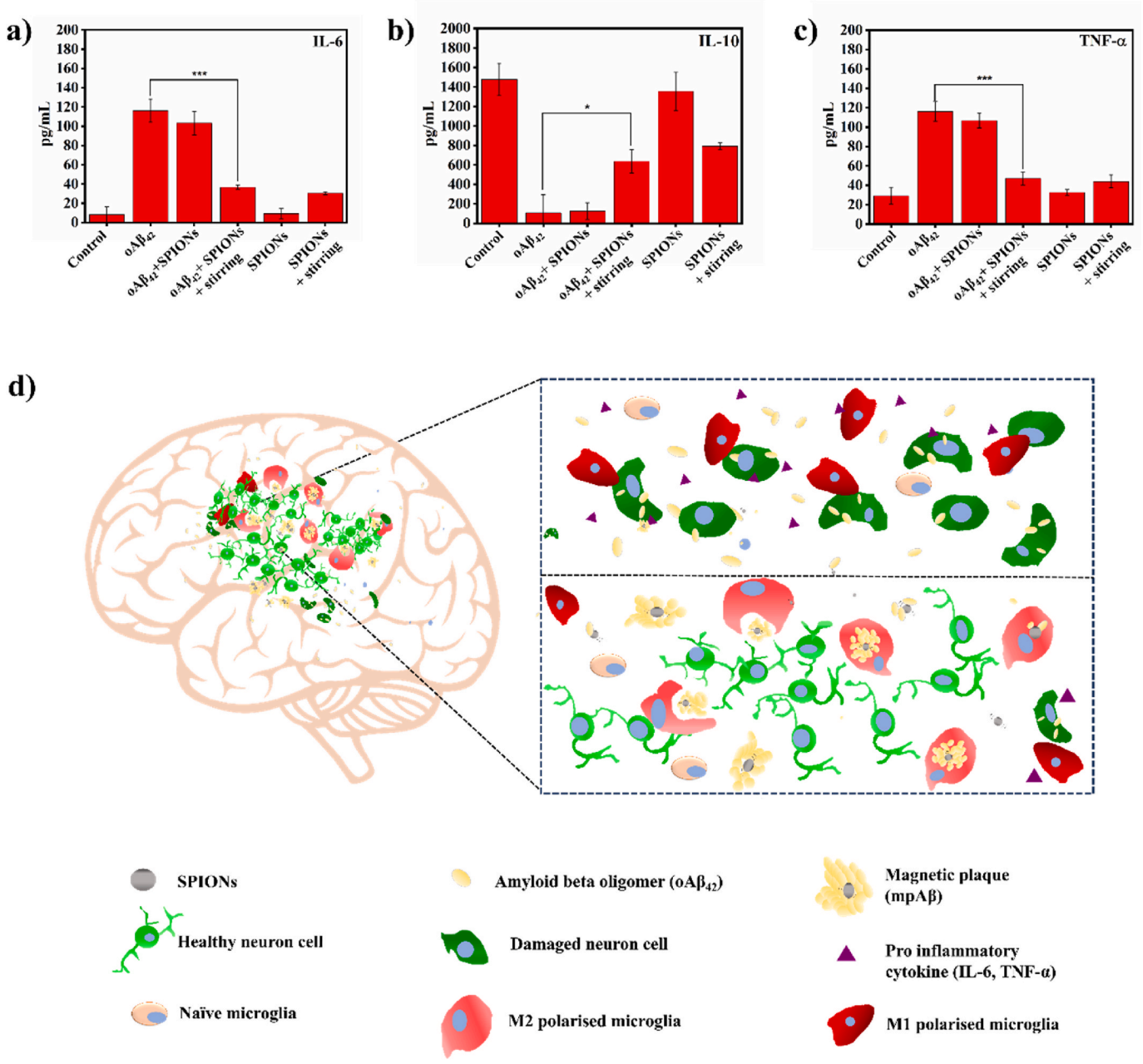

Fig. 5. Concentrations of IL-6 (a), IL-10 (b) and TNF-α (c) secretion from BV-2 cells receiving various treatments as determined by ELISA assay (n = 6). *p < 0.05, ***p < 0.001. d) Schematic of macrophage polarization with and without SPION magnetic stirring treatment. The naïve macrophages when are exposed to $oA\beta_{42}$ uptake undergo the M1 polarization. On the other hand, the magnetic stirring treatment with SPIONs causes the aggregation of $oA\beta_{42}$ into mpAβ. This aggregated form is then phagocytosed by microglial cells, leading to the polarization of brain macrophages into the M2 phenotype, thereby enhancing anti-inflammatory responses.

the macrophages into the M1 type while the magnetic stirring treatment that accretes oAβ_{42} into plaques results in an inhibition in the M1 polarization of microglia. These findings support the protective role of the SPION stirring treatment against oAβ_{42} mediated neuroinflammation and neuronal death in vitro [43]. In addition, the cell viability of N2a cells incubated for 24 h in the conditioned medium obtained from the co-culture of BV2 cells with oAβ_{42} with SPION stirring treatment was evaluated. The results are shown in Fig. S8c. The viability of N2a cells was somewhat reduced when being incubated with the conditioned medium harvested from the co-culture of BV2 cells with oAβ_{42}, indicating the increased cytotoxicity of the conditioned medium by the activation of microglia receiving the oAβ_{42} treatment. Nevertheless, the cytotoxicity of the conditioned medium was considerably alleviated by the SPION treatment conducted while the BV2 cells were co-incubated with oAβ_{42} species. In agreement with the aforementioned data, the oAβ_{42}-induced inflammation response from the microglia cells was largely reduced due to the facilitated accretion of oAβ_{42} species into large aggregates by the SPION stirring treatment, thereby reducing the release of the pro-inflammatory cytokines in the cultured medium of BV2 cells that are harmful against the neuron cells.

3.5. *Cognitive performance of AD mice by SPION stirring treatment*

The therapeutic efficacy of the SPION stirring treatment against AD in vivo was examined in terms of the evaluation of the memory and learning capability with and without the stirring treatment. The magnetic stirring treatment conducted on the AD mice is illustrated in Fig. S9a. The nesting behavior tests engaging a broad network of brain regions in mice have been frequently adopted to evaluate daily living skills of the AD mice. Fig. 6a shows that the healthy control group and the PBS group (the healthy mice receiving intracranial injection of PBS) shredded the cotton nestlets within 24 h and constructed the nest within 5 days. Similarly, the mice receiving the SPION stirring treatment in the absence of oAβ_{42} performed the nesting task successfully, signifying the absence of the cognitive disorder that was caused by the stirring treatment. By contrast, the mice in both the oAβ_{42} group and the oAβ_{42}+-SPIONs group (without stirring) shredded the cotton lint, but failed to construct the nest within 5 days, indicative of the impairment of the nesting capability with the oAβ_{42} treatment. The results clearly indicate that the oAβ_{42} species induces cognitive deficits and such deficits are not ameliorated by the presence of SPIONs without stirring. With the SPION magnetic stirring being performed, the oAβ_{42} treated mice became able to construct nests similar to the control group, revealing the capability of the SPION stirring strategy to accrete the oAβ_{42} via its agitation motion and hence alleviate the adverse effects caused by oAβ_{42}.

Barnes maze test was also employed to evaluate the capability of spatial learning and memory of oAβ_{42}-injected mice receiving the SPION stirring treatment. In the Barnes maze experiment, mice were trained to find a hidden chamber under the surface of a circular table. Light illumination was used in this task to induce the anxiety of mice and the motivation to find the hidden hole. As an additional motivation driver, food was hidden inside the dark box. The maze was divided into 4 quadrants and, among them, one quadrant was designed as the target by creating the hidden hole in the center along the quadrant rim (Fig. S9b). The mice were fasted for 8 h prior to the Maze test. The test was conducted for 5 consecutive days while the evaluation was performed daily. The time span and moving path that mice spent to find the hidden chamber was adopted as a measure of spatial learning and memory for mice receiving the oAβ_{42} intracranial injection with and without the SPION stirring treatment. As shown in Fig. 6b, the oAβ_{42} and the oAβ_{42}+SPIONs without stirring groups show appreciably reduced moving activity in the targeted quadrant compared to the control and the PBS group during the Barnes maze tests. This is ascribed to the impairment of the learning ability and/or memory as a result of the oAβ_{42} treatment. Nevertheless, the moving activity of the oAβ_{42}-injected mice after the SPION stirring treatment within the targeted quadrant was significantly restored. The quantified data showing the average time spans and moving lengths among different groups are presented in

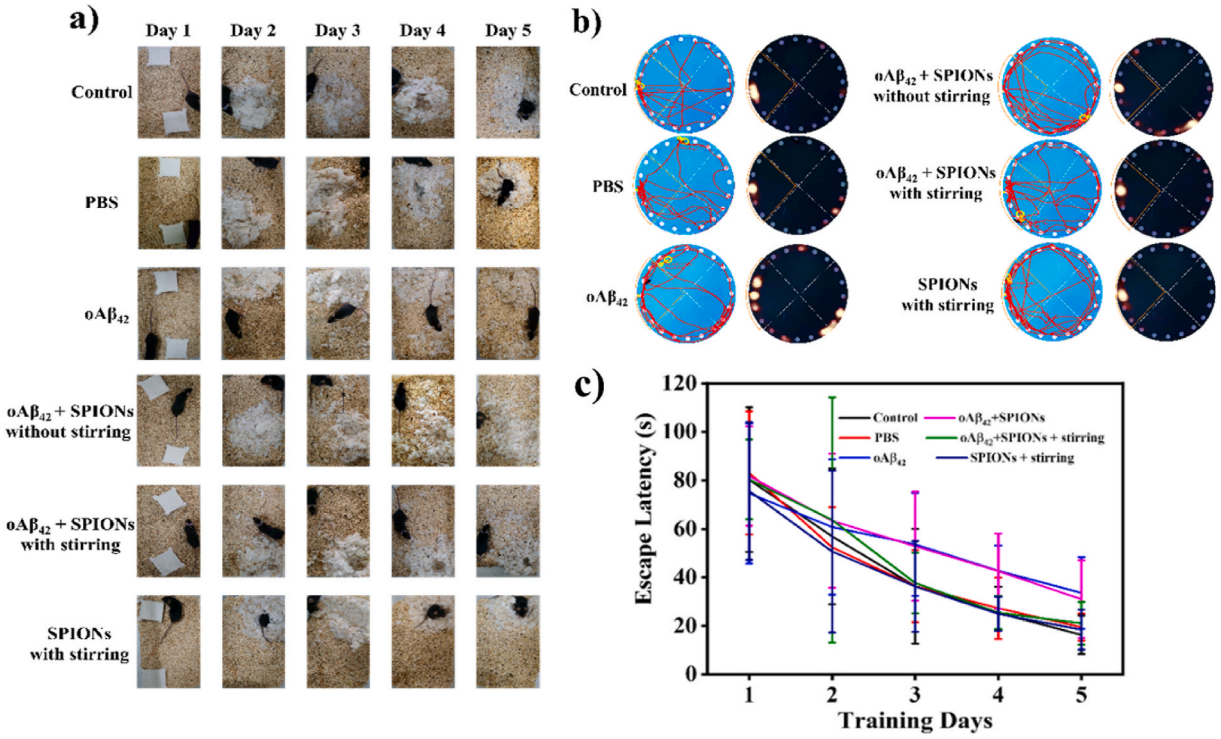

Fig. 6. (a) Nest construction behaviour of mice injected with oAβ_{42} and with or without SPION stirring treatments. Nesting materials were 2 pieces of cotton lint (5*5*0.5 cm*cm*cm) (n = 3 in each group). (b) Representative moving path of mice from different groups in the Barnes maze test (n = 3 in each group). (c) Time spans for mice receiving various treatments to find the hidden chamber in Barnes maze test.

Figs. S9c and S9d. As a result, Fig. 6c shows reduced time spans required to find the hidden chamber in the control and the PBS group compared to the oAβ_{42} and oAβ_{42}+SPION without stirring groups after 5-day training. The oAβ_{42}-injected mice exhibited learning and memory impairment by showing prolonged time required to find the hidden chamber. The treatment combining SPIONs with magnetic stirring appreciably alleviates the memory impairment of the oAβ_{42} -treated mice to an extent comparable to the control and PBS groups. It is worthy to note that the mice subjected to the SPION stirring without oAβ_{42} showed similar cognitive behavior and performance to the control group, indicating little damage in the cognitive ability caused by SPION stirring treatment. The Barnes maze examination clearly manifests the significant therapeutic effect of the SPION stirring treatment on inhibiting the loss in both memory and learning ability observed in the mice treated with oAβ_{42}.

3.6. *Ex vivo brain tissue studies*

With the therapeutic effect of the SPION stirring treatment being evaluated in terms of the alleviation of impaired cognitive performance of the oAβ_{42}-injected mice, the therapeutic efficacy of the treatment was further assessed with brain tissue staining of Aβ_{42} in different structures and AD-related markers. The mice were euthanized and the brain tissues were isolated. The formation of Aβ plaques was evaluated with CR and IHC (anti-fibril Aβ_{42} antibody) assay. The data are shown in Fig. 7a and S10a. From the both CR and IHC tissue staining of Aβ_{42}, it is obvious that the injection of oAβ_{42} can form npAβ in mice brain in support of successful formation of the AD model by intracranial injection of oAβ_{42}. The healthy mice used as the control without oAβ injection showed few aggregates in the brain. The SPION stirring treatment accelerates the agglomeration of oAβ_{42} and thus the formation of large plaques in the brain tissues. In the absence of the SPION stirring treatment, the brain tissues exhibited relatively smaller aggregates (npAβ) compared to those with the SPION stirring treatment as elucidated by both CR and IHC staining. Without magnetic stirring, the SPIONs are incapable to capture the oAβ species into mpAβ. Therefore, the signal intensity is comparable to that from the brain tissues only treated with oAβ_{42}. In AD, the Aβ molecules involved in the intricate processes with other AD-related species induce the dysregulation of calcium homeostasis and neurotoxicity [44]. Thus, Nissl staining has been developed and widely used to the pathologic detection of tissue damage by identifying the Nissl body of neuron cells mostly with immunocytochemistry staining in neural tissues [45]. Fig. 7b shows the images of the Nissl-stained hippocampus region of the mice brain receiving various treatments. With being treated with only oAβ_{42} species, the neurons were obviously decreased by showing weak signals highlighted in violet along with an increase in disconnection of neuron arrangement. The cell damage caused by oAβ_{42} was alleviated with the SPION stirring treatment to an extent comparable to the PBS group. Caspase 3 activity in the brain tissue was evaluated by IHC staining. The data are shown in Fig. 7c and S10b. It was observed that the oAβ_{42} significantly enhanced the caspase 3 level in brain tissues, indicating an increase in the cell number undergoing apoptosis compared to the control group. As expected, the SPION stirring treatment over the oAβ_{42} injected mice significantly reduced the apoptosis of neurons as reflected by the decrease of the caspase 3 signal intensity in brain tissues. The results corroborate that the SPION stirring treatment protects the neuronal cells from damage caused by the oAβ_{42} toxicity.

The accretion of oAβ_{42} by the SPION stirring treatment into SPIONs-contained aggregates prevents the oAβ_{42} species from cellular uptake by neurons, thereby reducing its toxicity toward neuronal cells. It is readily understood that the inflammatory responses of the brain tissues induced by the oAβ_{42} species include the reactions from microglia. The recruitment of microglial cells was thus evaluated in brain tissues involved with different treatments. Iba1, a typical marker for microglial cells, was used to evaluate the presence of the cells in the brain tissues. As shown in Fig. 7d, the microglia level in brain tissues treated only with oAβ_{42} is appreciably enhanced compared to the control and PBS groups, being as a characteristic sign of tissue inflammation. Nevertheless, the signal intensity of Iba1 staining on the oAβ_{42} brain tissues was much reduced after the SPION stirring treatment, to an extent comparable to the control group, manifesting the reduction in both neuronal inflammation and microglial recruitment to the inflammatory area. The quantified data are illustrated in Fig. S10c. CD68 was adopted as a marker of activated microglia for the fluorescence staining in brain tissues to evaluate the level and activity of microglia after various treatments. The results illustrated in Fig. 7e indicate the pronounced effect of the SPION stirring treatment to suppress the inflammation caused by oAβ_{42}. In the

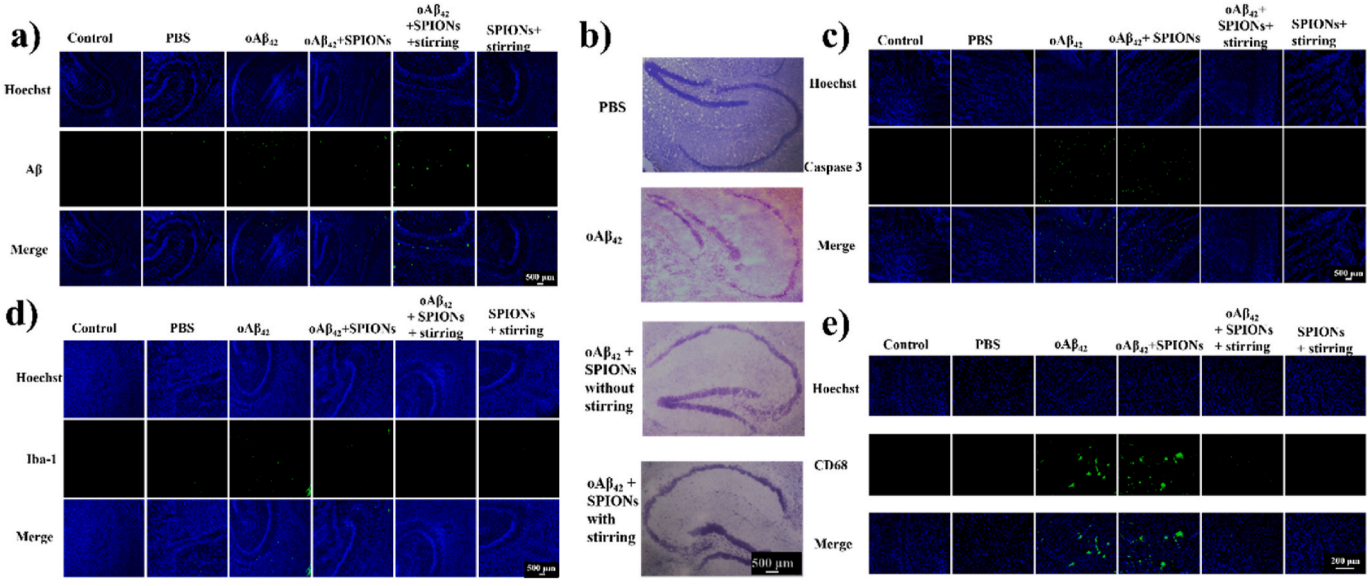

Fig. 7. (a) IHC staining (anti-fibril Aβ_{42} as the primary antibody) of Aβ_{42} aggregates in brain tissues harvested from mice receiving various treatments. Cell nuclei were stained with Hoechst 33342. (b) Images of the Nissl-stained brain hippocampus region of the mice receiving various treatments. (c) Images identifying IHC staining of caspase 3 in brain tissues with various treatments. (d) Images of brain tissues after various treatments with IHC staining on Iba1 as a marker to signify the microglia level. (e) Images of brain tissues receiving various treatments with fluorescence staining of CD68 to represent the level of activated microglia.

absence of the SPION stirring treatment, the oAβ_{42} group exhibited enhanced CD68 signal intensity in brain tissues, suggesting that microglial cells were recruited and activated to take part in the inflammation reactions as one of key factors inducing the pathogenesis of AD. The SPION stirring treatment induces the accretion of oAβ_{42} and thus protect the cells from neurotoxicity of oAβ_{42} and prevent microglial cells from activation that intensifies inflammation.

3.7. *Effects of stirring treatment on astrocytes in AD mice*

Astrocytes are one of key regulators in the inflammatory responses in brain. Reactive astrogliosis has been observed in AD and is marked by an increase in glial fibrillary acidic protein (GFAP) [46]. In this work, the IHC staining of GFAP was conducted on the sections of brain tissues receiving different treatments. The data are illustrated in Fig. 8a and b. The groups treated with oAβ_{42} alone and SPION+oAβ_{42} without stirring treatment exhibited enhanced fluorescence signals, indicating increased GFAP expression by oAβ_{42} induced astrocyte activation. This also leads to neuroinflammation and neuronal damage in the mouse brain. Nevertheless, following the SPION stirring treatment, the GFAP expression was reduced, suggesting that the treatment accretes oAβ_{42} into large magnetic plaques, which is the key step in reducing the stimulation of astrogliosis. Excitatory amino acid transporter-2 (EAAT-2) is one of the major glutamate transporters expressed predominantly in astroglia cells (astrocytes). Thus, the activation of astrocytes was also examined in terms of the expression of EAAT-2. In agreement with the data from the tissue GFAP staining, the oAβ_{42} treatment enhanced the EAAT-2 signal intensity in brain tissue, confirming the activation of astrocytes with the presence of oAβ_{42} (Fig. S11a). The effect of the SPION stirring treatment on suppressing the activation of astrocytes was also observed in a similar manner to the GFAP examination. It has been well known that microglia and astrocytes are not only activated and induced to release chemokines and cytokines in the presence of oAβ_{42}, but these cells also react to pro-inflammatory

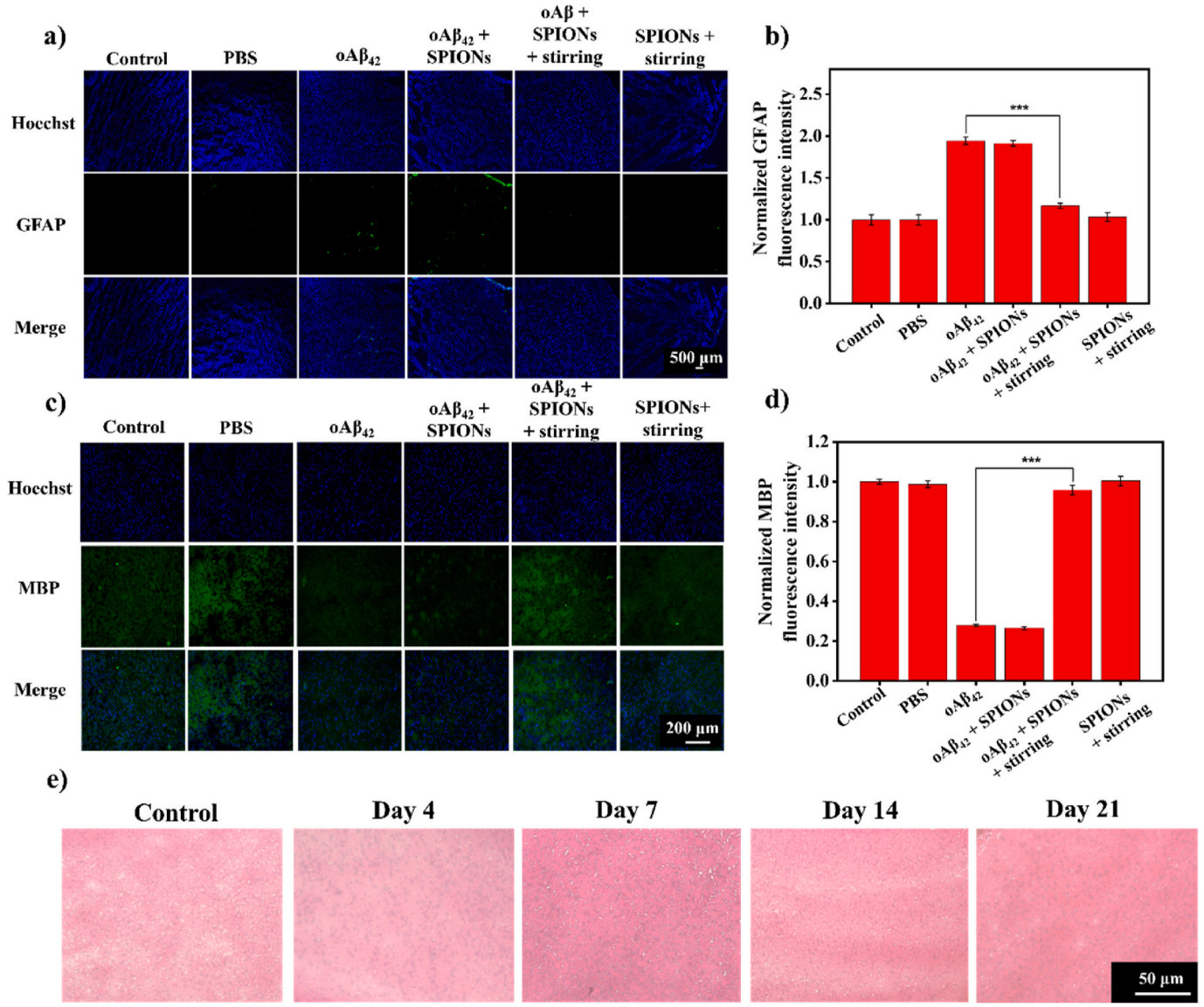

Fig. 8. (a) LSCM images of brain tissue sections with IHC staining (in green) of GFAP as the astrocyte activation marker from mice receiving different treatments. Cell nuclei were stained with Hoechst 33342 (blue). Scale bar 500 μm. (b) Quantified data also included. (n = 5) (c) LSCM images of brain tissue sections with IHC staining (in green) of MPB as a marker for oligodendrocyte differentiation and myelination from mice receiving different treatments. Scale bar 200 μm (d) Quantified data are also included, (n = 5). e). H&E staining of brain tissues over various time intervals after being subjected to the SPION stirring treatment at 2500 rpm for 30 min. Scale bar 50 μm. Samples were analyzed with one-way ANOVA. *p < 0.05, **p < 0.01, ***p < 0.001. Error bars represent mean ± s.d. (n = 5 for all groups). (For interpretation of the references to colour in this figure legend, the reader is referred to the Web version of this article.)

cytokines and produce more Aβ species in response [47,48]. The SPION stirring approach obviously reduces the activation of these cells and protects the cells from further complications as aforementioned. Oligodendrocytes and myelin present in the central nervous system also provide metabolic and trophic supports for axons and their damage and dysfunction plays a crucial role to axonal death and neurodegeneration, which are key features of AD. Myelin basic protein (MBP) is a major myelin constituent produced by oligodendrocytes. Expression of MBP has been often considered a marker for oligodendrocyte differentiation and myelination [49]. The IHC staining of the MBP from the brain tissue sections after various treatments was conducted. The results are illustrated in Fig. 8c and d. The signal intensity of MBP was significantly reduced with intracranial administration of $oA\beta_{42}$ in the mice brain. Nevertheless, the SPION stirring treatment prevents the oligodendrocytes from the $oA\beta_{42}$ induced damage, thus maintaining the expression of MBP to an extent similar to the positive control group. Based upon the evaluation of various markers in brain tissues, it is evident that $oA\beta_{42}$ induces significant cytotoxicity toward neuron cells and aggregates to form npAβ inside the brain tissues. The deposition of $oA\beta_{42}$ increases the activation of microglial cells and astrocytes in the brain, thereby promoting the inflammatory cytokines secretion and inducing damage to the neuron cells as the key features of AD. However, the SPION stirring treatment protects the neuron cells from the uptake of $oA\beta_{42}$ by capturing them into large magnetic plaques. As a consequence, the activation of microglia and astrocytes by $oA\beta_{42}$ is appreciably reduced. The tissue damage caused simply by the SPION stirring treatment was examined by the H&E staining of the brain tissues. The images illustrated in Fig. 8e on the brain tissues (hippocampus regions) receiving the SPION stirring treatment harvested over various time intervals ($n = 3$ at each time interval) signify negligible tissue damage or cell death up to 21 days. The harvested brain tissues were also subjected to Prussian blue staining to identify the presence of SPIONs with time. As shown in Fig. S12a, the Prussian blue staining of the iron oxide NPs in the tissue sections was observed over 4 days after the SPION stirring treatment while SPIONs were barely detected since day 7 and after, implying the almost complete degradation of the SPIONs in brain tissues. Generally, the SPIONs can dissolve into iron ions (Fe^{2+} and Fe^{3+}) under acidic conditions typically found in subcellular lysosomes. Previous reports investigating the uptake and potential toxicity of iron oxide NPs using microglial cells have found negligible cytotoxic effect of the NPs on brain macrophages and confirmed their elimination [50,51]. It is noteworthy that the body weight of mice remains relatively unchanged after the stirring treatment (Fig. S12b) over 21 days, suggesting that the therapy modality does not elicit severe side effects.

4. Conclusions

In a nutshell, citric acid coated SPIONs serving in this work as superparamagnetic nanospinners for capturing and accretion of $oA\beta_{42}$ with the aid of magnetic field was developed. The in vitro and in vivo experiments proved the efficacy of the SPION stirring treatment for rapid capturing of toxic $oA\beta_{42}$ and their accretion into insoluble, less cytotoxic, and nonpathogenic mpAβ. In spite of the inherent toxicity of $oA\beta_{42}$ toward neurons with reduced viability and impaired cellular functions, the SPION stirring treatment acts as an effective barrier against the uptake of $oA\beta_{42}$ by neuronal cells and thus protects these cells from the $oA\beta_{42}$ damage by rapidly accreting them into large plaques under a rotating magnetic field. Neither SPIONs alone nor the combination with the stirring treatment is harmful to the neurons, highlighting the advantages of the strategy in the absence of mechanical ablation against the treated cells. The in vitro study showed that the large mpAβ plaques formed by accretion of $oA\beta_{42}$ was cleared by microglial cells, but not neurons. It was found that the microglia after the uptake of mpAβ showed reduced production of pro-inflammatory cytokines alongside the increase of anti-inflammatory cytokines, strongly suggesting the polarization of macrophages (microglia) from M1 to M2 phenotype. Such M2 polarization also accounts in part for the enhanced uptake of the mpAβ by the microglia. The in vivo study also revealed that the intracranial injection of $oA\beta_{42}$ into mouse brain induced learning and memory impairment, ensuring the implications of AD. The mice receiving SPION stirring treatment showed significantly improved cognitive performance. The brain tissue analyses also clearly manifested the alleviation in neurotoxicity caused by $oA\beta_{42}$ and reduction in the activation of microglia and astrocytes as a key step to intensify AD-featured inflammation. This drug-free therapeutic strategy developed in this study showed its promise for the AD treatment although further detailed studies on the treatment parameters, such as the dose of SPIONs, the stirring duration, the stirring rate and the treatment frequency, are required with transgenic AD animal models. In addition, administration of SPIONs was conducted by intracranial injection for the treatment of the AD mice using a stereotaxic instrument in this work, which might be feasible for future clinical application under careful and precise monitoring with professional clinicians since blood-brain barrier limits their use by intravenous administration. Nevertheless, this study focuses mainly on the proof of this strategy and more detailed therapeutic evaluations from animal models are essential, in particular, to validate the biosafety of the treatment.

Data and materials availability

All data are available in the main text or the supplementary materials.

CRediT authorship contribution statement

Arjun Sabu: Writing – review & editing, Writing – original draft, Visualization, Validation, Methodology, Formal analysis, Conceptualization. **Yu Ching Huang:** Visualization, Validation, Project administration, Investigation, Formal analysis, Conceptualization. **Ramalingam Sharmila:** Writing – review & editing, Writing – original draft, Visualization, Validation, Formal analysis. **Chih-Yuan Sun:** Visualization, Validation, Software, Formal analysis, Data curation, Conceptualization. **Min-Ying Shen:** Visualization, Validation, Methodology, Formal analysis. **Hsin-Cheng Chiu:** Writing – review & editing, Writing – original draft, Visualization, Validation, Supervision, Project administration, Methodology, Investigation, Funding acquisition, Formal analysis, Conceptualization.

Declaration of competing interest

The authors whose names are listed immediately below certify that they have declare **no conflict of interest** in the subject matter or materials discussed in this manuscript.

Data availability

Data will be made available on request.

Acknowledgments

We acknowledge the financial supports by the National Science and Technology Council, Taiwan (NSTC 111-2314-B-007-001-MY3, NSTC 110-2221-E-007-018-MY3 and NSTC 113-2221-E-039-009), China Medical University Hsinchu Hospital, Taiwan (CMUHCH-DMR-113-019), National Tsing Hua University, Taiwan (110Q2537E1), and Taoyuan General Hospital, Taiwan (PTC110005).

Appendix A. Supplementary data

Supplementary data to this article can be found online at https://doi.org/10.1016/j.mtbio.2024.101213.

References

[1] A. Gustavsson, N. Norton, T. Fast, L. Frölich, J. Georges, D. Holzapfel, T. Kirabali, P. Krolak-Salmon, P.M. Rossini, M.T. Ferretti, L. Lanman, A.S. Chadha, W.M. van der Flier, Global estimates on the number of persons across the Alzheimer's disease continuum, Alzheimer's and dementia, Alzheimer's Dement 19 (2023) 658–670.

[2] E. Rudnicka-Drożak, P. Drożak, G. Mizerski, T. Zaborowski, B. Ślusarska, G. Nowicki, M. Drożak, Links between COVID-19 and Alzheimer's disease—what do we already know? Int. J. Environ. Res. Publ. Health 20 (2023) 2146.

[3] E. Nichols, J.D. Steinmetz, S.E. Vollset, K. Fukutaki, et al., Estimation of the global prevalence of dementia in 2019 and forecasted prevalence in 2050: an analysis for the global burden of disease study 2019, Lancet Public Health 7 (2022) 105–125.

[4] P. Madhu, S. Mukhopadhyay, Distinct types of amyloid-β oligomers displaying diverse neurotoxicity mechanisms in Alzheimer's disease, J. Cell. Biochem. 122 (2021) 1594–1608.

[5] F. Panza, M. Lozupone, G. Logroscino, B.P. Imbimbo, A critical appraisal of amyloid-β-targeting therapies for Alzheimer disease, Nat. Rev. Neurol. 15 (2019) 73–88.

[6] J.P. Cleary, D.M. Walsh, J.J. Hofmeister, G.M. Shankar, M.A. Kuskowski, D. J. Selkoe, K.H. Ashe, Natural oligomers of the amyloid-β protein specifically disrupt cognitive function, Nat. Neurosci. 8 (2005) 79–84.

[7] S. Merlo, S.F. Spampinato, M.A. Sortino, Early compensatory responses against neuronal injury: a new therapeutic window of opportunity for Alzheimer's disease? CNS Neurosci, Ther 25 (2019) 5–13.

[8] M. Sciaccaluga, A. Megaro, G. Bellomo, G. Ruffolo, M. Romoli, E. Palma, C. Costa, An unbalanced synaptic transmission: cause or consequence of the amyloid oligomers neurotoxicity? Int. J. Mol. Sci. 22 (2021) 5991.

[9] C. Lindberg, M.L.B. Selenica, A. Westlind-Danielsson, M. Schultzberg, β-Amyloid Protein structure determines the nature of cytokine release from rat microglia, J. Mol. Neurosci. 27 (2005) 1–12.

[10] C.M. Sondag, G. Dhawan, C.K. Combs, Beta amyloid oligomers and fibrils stimulate differential activation of primary microglia, J. Neuroinflammation 6 (2009) 1.

[11] J.M. Crain, M. Nikodemova, J.J. Watters, Microglia express distinct M1 and M2 phenotypic markers in the postnatal and adult central nervous system in male and female mice, J. Neurosci. Res. 91 (2013) 1143–1151.

[12] V. Calsolaro, P. Edison, Neuroinflammation in Alzheimer's disease: current evidence and future directions, Alzheimer's Dement. 12 (2016) 719–732.

[13] M.A. Meraz-Ríos, D. Toral-Rios, D. Franco-Bocanegra, J. Villeda-Hernández, V. Campos-Peña, Inflammatory process in Alzheimer's disease, Front. Integr, Neurosci 7 (2013).

[14] Y. Tang, W. Le, Differential roles of M1 and M2 microglia in neurodegenerative diseases, Mol. Neurobiol. 53 (2016) 1181–1194.

[15] W. Yang, Q. Wu, C. Yuan, J. Gao, M. Xiao, M. Gu, J. Ding, G. Hu, Aquaporin-4 mediates astrocyte response to β-amyloid, Mol. Cell. Neurosci. 49 (2012) 406–414.

[16] M.M. Varnum, T. Ikezu, The classification of microglial activation phenotypes on neurodegeneration and regeneration in alzheimer's disease brain, Arch. Immunol. Ther. Exp. 60 (2012) 251–266.

[17] B. Parajuli, Y. Sonobe, H. Horiuchi, H. Takeuchi, T. Mizuno, A. Suzumura, A. Oligomeric amyloid β induces IL-1β processing via production of ROS: implication in Alzheimer's disease, Cell Death Dis. 4 (2013) 975.

[18] C. Gao, J. Jiang, Y. Tan, S. Chen, Microglia in neurodegenerative diseases: mechanism and potential therapeutic targets, Signal Transduct. Targeted Ther. 8 (2023) 359.

[19] S.R. Meier, S. Syvänen, G. Hultqvist, X.T. Fang, S. Roshanbin, L. Lannfelt, U. Neumann, D. Sehlin, Antibody-based in vivo PET imaging detects amyloid-ß reduction in Alzheimer transgenic mice after BACE-1 inhibition, J. Nucl. Med. 59 (2018) 1885–1891.

[20] M.A. Maia, E. Sousa, BACE-1 and γ-Secretase as therapeutic targets for Alzheimer's disease, Pharmaceuticals 12 (2019) 41.

[21] K. Hou, J. Zhao, H. Wang, B. Li, K. Li, X. Shi, K. Wan, J. Ai, J. Lv, D. Wang, Q. Huang, H. Wang, Q. Cao, S. Liu, Z. Tang, Chiral gold nanoparticles enantioselectively rescue memory deficits in a mouse model of Alzheimer's disease, Nat. Commun. 11 (2020) 4790.

[22] J. Jang, C.B. Park, Magnetoelectric dissociation of Alzheimer's β-amyloid aggregates, Sci. Adv. 8 (2022) 1675.

[23] T.F. Beckhauser, J. Francis-Oliveira, R. De Pasquale, Reactive oxygen species: physiological and physiopathological effects on synaptic plasticity, J. Exp. Neurosci. (2016) 23–48.

[24] D. Lee, D. Park, I. Kim, S.W. Lee, W. Lee, K.S. Hwang, J.H. Lee, G. Lee, D.S. Yoon, Plasmonic nanoparticle amyloid corona for screening Aβ oligomeric aggregate-degrading drugs, Nat. Commun. 12 (2021) 639.

[25] Y.C. Tsai, J.C. Luo, T.I. Liu, I.L. Lu, M.Y. Shen, C.Y. Chuang, C.S. Chern, H.C. Chiu, Capturing amyloid-β oligomers by stirring with microscaled iron oxide stir bars into magnetic plaques to reduce cytotoxicity toward neuronal cells, Nanomaterials 10 (2020) 1284.

[26] K. Wu, A. Mohsin, W.Q. Zaman, Z. Zhang, W. Guan, M. Chu, Y. Zhuang, M. Guo, J Urchin-like magnetic microspheres for cancer therapy through synergistic effect of mechanical force, photothermal and photodynamic effects, Nanobiotechnol 20 (2022) 224.

[27] D.H. Kim, E.A. Rozhkova, I.V. Ulasov, S.D. Bader, T. Rajh, M.S. Lesniak, V. Novosad, Biofunctionalized magnetic-vortex microdiscs for targeted cancer-cell destruction, Nat. Mater. 9 (2010) 165–171.

[28] N.H. Khan, M. Mir, E.E. Ngowi, U. Zafar, M.M.A.K. Khakwani, S. Khattak, Y. K. Zhai, E.S. Jiang, M. Zheng, S.F. Duan, J.S. Wei, D.D. Wu, X.Y. Ji, Nanomedicine: a promising way to manage Alzheimer's disease, Front. Bioeng. Biotechnol. 9 (2021 Apr 9) 630055.

[29] T. Yin, Y. Liu, B. He, B. Gong, J. Chu, C. Gao, W. Liang, M. Hao, W. Sun, J. Zhuang, J. Gao, Y. Yin, Cell primitive-based biomimetic nanomaterials for Alzheimer's disease targeting and therapy, Mater. Today Bio 22 (2023) 100789.

[30] M. Mahmoudi, S. Sant, B. Wang, S. Laurent, T. Sen, Superparamagnetic iron oxide nanoparticles (SPIONs): development, surface modification and applications in chemotherapy, Adv. Drug Deliv. Rev. 63 (2011) 24–46.

[31] S. Luo, C. Ma, M.Q. Zhu, W.N. Ju, Y. Yang, X. Wang, development, surface modification and applications in chemotherapy, Front. Cell. Neurosci. 14 (2020).

[32] W.C. Huang, I.L. Lu, W.H. Chiang, Y.W. Lin, Y.C. Tsai, H.H. Chen, C.W. Chang, C. S. Chiang, H.C. Chiu, Tumortropic adipose-derived stem cells carrying smart nanotherapeutics for targeted delivery and dual-modality therapy of orthotopic glioblastoma, J. Contr. Release 254 (2017) 119–130.

[33] K.N. Dahlgren, A.M. Manelli, W. Blaine Stine, L.K. Baker, G.A. Krafft, M.J. Ladu, Oligomeric and fibrillar species of amyloid-β peptides differentially affect neuronal viability, J. Biol. Chem. 277 (2002) 32046–32053.

[34] M.P. Lambert, K.L. Viola, B.A. Chromy, L. Chang, T.E. Morgan, J. Yu, D.L. Venton, G.A. Krafft, C.E. Finch, W.L. Klein, Vaccination with soluble Aβ Oligomers generates toxicity-neutralizing antibodies, J. Neurochem. 79 (2001) 595–605.

[35] Z. Razmara, S. Saheli, V. Eigner, M. Dusek, Synthesis, crystal structure and magnetic properties of a new tri-nuclear iron (II, III) complex, a precursor for the preparation of superparamagnetic Fe_3O_4 nanoparticles applicable in the removal of Cd^{2+}, Appl. Organometal. Chem 33 (2019) 4880.

[36] M. Biancalana, S. Koide, Molecular mechanism of Thioflavin-T binding to amyloid fibrils, Biochim. Biophys. Acta 7 (2010) 1405–1412.

[37] M. Ahmed, J. Davis, D. Aucoin, T. Sato, S. Ahuja, S. Aimoto, J.I. Elliott, W.E. Van Nostrand, S.O. Smith, Structural conversion of neurotoxic Amyloid- β 1-42 oligomers to fibrils, Nat. Struct. Mol. Biol. 17 (2010) 561–567.

[38] Y. Zhang, H. Chen, R. Li, K. Sterling, W. Song, Amyloid β-based therapy for Alzheimer's disease: challenges, successes and future, Signal Transduct. Target. Ther. 8 (2023) 248.

[39] H. Kadowaki, H. Nishitoh, F. Urano, C. Sadamitsu, A. Matsuzawa, K. Takeda, H. Masutani, J. Yodoi, Y. Urano, T. Nagano, H. Ichijo, Amyloid β Induces Neuronal cell death through ROS-mediated ASK1 activation, Cell Death Differ. 12 (2005) 19–24.

[40] X.J. Han, Y.Y. Hu, Z.J. Yang, L.P. Jiang, S.L. Shi, Y.R. Li, M.Y. Guo, H.L. Wu, Y. Y. Wan, Amyloid β-42 induces neuronal apoptosis by targeting mitochondria, Mol. Med. Rep. 16 (2017) 4521–4528.

[41] Z. Yu, Q. Li, J. Wang, Y. Yu, Y. Wang, Q. Zhou, P. Li, Reactive oxygen species-related nanoparticle toxicity in the biomedical field, Nanoscale Res. Lett. 15 (2020) 115.

[42] M. Fujikura, N. Iwahara, S. Hisahara, J. Kawamata, A. Matsumura, K. Yokokawa, T. Saito, T. Manabe, T. Matsushita, S. Suzuki, S. Shimohama, CD14 and Toll-Like receptor 4 promote fibrillar Aβ 42 uptake by microglia through a clathrin-mediated pathway, J. Alzheimer's Dis. 68 (2019) 867–884.

[43] F. Leng, P. Edison, Neuroinflammation and Microglial Activation in Alzheimer disease: where do we go from here? Nat. Rev. Neurol. 17 (2021) 157–172.

[44] M. Arbel-Ornath, E. Hudry, J.R. Boivin, T. Hashimoto, S. Takeda, K.V. Kuchibhotla, S. Hou, C.R. Lattarulo, A.M. Belcher, N. Shakerdge, P.B. Trujillo, A. Muzikansky, R. A. Betensky, B.T. Hyman, B.J. Bacskai, Soluble oligomeric amyloid-β induces calcium dyshomeostasis that precedes synapse loss in the living mouse, Brain.Mol. Neurodegener. 12 (2017) 27.

[45] A. Kádár, G. Wittmann, Z. Liposits, C. Fekete, Improved method for combination of immunocytochemistry and Nissl staining, J. Neurosci. Methods 184 (2009) 115–118.

[46] W. Kamphuis, J. Middeldorp, L. Kooijman, J.A. Sluijs, E.J. Kooi, M. Moeton, M. Freriks, M.R. Mizee, E.M. Hol, Glial fibrillary acidic protein isoform expression in plaque related astrogliosis in Alzheimer's disease, Neurobiol. Aging 35 (2014) 492–510.

[47] Y. Cai, J. Liu, B. Wang, M. Sun, H. Yang, Microglia in the neuroinflammatory pathogenesis of Alzheimer's disease and related therapeutic targets, Front. Immunol. 13 (2022).

[48] L. Montoliu-Gaya, S.D. Mulder, M.A.C. Herrebout, J.C. Baayen, S. Villegas, R. Veerhuis, Aβ-oligomer uptake and the resulting inflammatory response in adult human astrocytes are precluded by an anti-Aβ single chain variable fragment in combination with an apoE mimetic peptide, Mol. Cell. Neurosci. 89 (2018) 49–59.

[49] N. Zečević, A. Andjelković, J.M. Matthieu, M. Tosić, Dev. Myelin basic protein immunoreactivity in the human embryonic CNS, Brain Res. 105 (1998) 97–108.

[50] E.M. Luther, C. Petters, F. Bulcke, A. Kaltz, K. Thiel, U. Bickmeyer, R. Dringen, Endocytotic uptake of iron oxide nanoparticles by cultured brain microglial cells, Acta Biomater. 9 (2013) 8454–8465.

[51] C.S. Lewis, L. Torres, J.T. Miyauchi, C. Rastegar, J.M. Patete, J.M. Smith, S. S. Wong, S.E. Tsirka, Absence of cytotoxicity towards microglia of iron oxide (α-Fe2O3) nanorhombohedra, Toxicol. Res. 5 (2016) 836–847.